

1 **Soil frost-enabled soil moisture precipitation feedback**  
2 **over northern high latitudes**

3 **Stefan Hagemann<sup>1\*</sup>, Tanja Blome<sup>1</sup>, Altug Ekici<sup>2</sup> and Christian Beer<sup>3</sup>**

4 <sup>1</sup> Max-Planck-Institut für Meteorologie, Bundesstr. 53, 20146 Hamburg, Deutschland,  
5 \* Tel.: +49 40 4117 3101, Email: stefan.hagemann@mpimet.mpg.de

6 <sup>2</sup> Earth System Sciences, Laver Building, University of Exeter, Exeter, UK

7 <sup>3</sup> Department of Environmental Science and Analytical Chemistry (ACES) and Bolin Centre  
8 for Climate Research, Stockholm University, Stockholm, Sweden.

9

10

11 **Abstract**

12 Permafrost or perennially frozen ground is an important part of the terrestrial cryosphere;  
13 roughly one quarter of Earth's land surface is underlain by permafrost. The currently observed  
14 global warming is most pronounced in the Arctic region and is projected to persist during the  
15 coming decades due to anthropogenic CO<sub>2</sub> input. This warming will certainly have effects on  
16 the ecosystems of the vast permafrost areas of the high northern latitudes. The quantification  
17 of such effects, however, is still an open question. This is partly due to the complexity of the  
18 system, including several feedback mechanisms between land and atmosphere. In this study  
19 we contribute to increasing our understanding of such land-atmosphere interactions using an  
20 Earth system model (ESM) which includes a representation of cold region physical soil  
21 processes, especially the effects of freezing and thawing of soil water on thermal and  
22 hydrological states and processes. The coupled atmosphere-land models of the ESM of the  
23 Max Planck Institute for Meteorology, MPI-ESM, have been driven by prescribed observed  
24 SST and sea ice in an AMIP2-type setup with and without newly implemented cold region  
25 soil processes. Results show a large improvement in the simulated discharge. On one hand  
26 this is related to an improved snowmelt peak of runoff due to frozen soil in spring. On the  
27 other hand a subsequent reduction of soil moisture enables a positive feedback to precipitation  
28 over the high latitudes, which reduces the model's wet biases in precipitation and  
29 evapotranspiration during the summer. This is noteworthy as soil moisture – atmosphere  
30 feedbacks have previously not been in the research focus over the high latitudes. These results  
31 point out the importance of high latitude physical processes at the land surface for the regional  
32 climate.

33 **Keywords:** Soil moisture – precipitation feedback, soil water freezing, permafrost regions,  
34 global climate modelling, high latitudes

## 35      **1 Introduction**

36      Roughly one quarter of the northern hemisphere terrestrial land surface is underlain by  
37      permafrost (Brown et al., 1997; French, 1990), which is defined as ground that is at or below  
38      zero degrees Celsius for more than two consecutive years. Permafrost soils build a globally  
39      relevant carbon reservoir as they store large amounts of deep-frozen organic material with  
40      high carbon contents (Ping et al., 2008) leading to a total pan-Arctic estimate of 1300 Pg of  
41      soil carbon (C) in these areas (Hugelius et al., 2014), which is twice the amount of the  
42      atmosphere's content. Moreover, the high northern latitudes are one of the critical regions of  
43      anthropogenic climate change, where the observed warming is clearly above average due to  
44      the so-called Arctic Amplification (Solomon et al., 2007; ACIA, 2005). Climate model  
45      simulations project this trend to continue (Serreze and Barry, 2011). The combination of the  
46      high C stocks in sub-arctic and arctic soils with the pronounced warming in the affected  
47      regions could thus lead to a positive biogeochemical feedback through the release of formerly  
48      trapped, 'deep-frozen' C into the atmosphere, when near-surface permafrost thaws. For the  
49      thawed soils and their biogeochemistry, it is decisive whether dry or wet conditions  
50      predominate: Aerobic decomposition is relatively fast and leads to the release of CO<sub>2</sub>, while  
51      anaerobic decomposition is much slower and leads to the release of CH<sub>4</sub> as the main product  
52      of the combustion of organic soil material. CH<sub>4</sub> is a much more potent greenhouse gas, but  
53      has a shorter lifetime of about 10 years after which it is converted to CO<sub>2</sub> by oxidation.  
54      Therefore, not only the soil's temperature, but also its moisture status are important for the  
55      assessment of the biogeochemical response to climatic conditions, and thus should be  
56      represented in climate or Earth System models in a realistic and process-based manner. Thus,  
57      the adequate representation of permafrost hydrology is a necessary and challenging task in  
58      Earth system modelling.

59 Hagemann et al. (2013a) described relevant hydrological processes that occur in permafrost  
60 areas and that should preferably be represented in models simulating interactions of  
61 permafrost hydrology with vegetation, climate and the carbon cycle. The current state of the  
62 representation of processes in general circulation models (GCMs) or Earth system models  
63 (ESMs) can be obtained by systematic model intercomparison through the various climate  
64 model intercomparison projects (CMIPs; Meehl et al., 2000) that have a long history within  
65 the climate modelling community. Results from CMIPs provide a good overview on the  
66 respective state of ESM model accuracy and performance. Koven et al. (2012) analysed the  
67 performance of ESMs from the most recent CMIP5 exercise over permafrost areas. They  
68 found that the CMIP5 models have a wide range of behaviours under the current climate, with  
69 many failing to agree with fundamental aspects of the observed soil thermal regime at high  
70 latitudes. This large variety of results originates from a substantial range in the level of  
71 complexity and advancement of permafrost-related processes implemented in the CMIP5  
72 models (see, e.g., Hagemann et al., 2013a), whereas most of these models do not include  
73 permafrost specific processes, not even the most basic process of freezing and thawing of soil  
74 water. Due to missing processes and related deficiencies of their land surface schemes,  
75 climate models often show substantial biases in hydrological variables over high northern  
76 latitudes (Luo et al., 2003; Swenson et al., 2012). Moreover, the land surface  
77 parameterizations used in GCMs usually do not adequately resolve the soil conditions (Walsh  
78 et al., 2005). The parameterizations often rely on either point measurements or on information  
79 derived from satellite data. Therefore, large efforts are ongoing to extend ESMs in this  
80 respect, in order to improve simulated soil moisture profiles and associated ice contents, river  
81 discharge, surface and sub-surface runoff. The ESM improvement over permafrost areas was,  
82 e.g., one of the research objectives of the European Union Project PAGE21  
83 ([www.page21.org](http://www.page21.org)).

84 The most basic process in permafrost areas is the seasonal freezing and thawing of soil water  
85 in the presence of continuously frozen ground below a certain depth. The response of the soil  
86 to freezing leads to specific variations in the annual cycle of soil hydrology. Frozen ground  
87 and snow cover also influence rainfall-runoff partitioning, the timing and magnitude of spring  
88 runoff, and the amount of soil moisture that subsequently is available for evapotranspiration  
89 in spring and summer (Beer et al., 2006; Beer et al., 2007; Koren et al., 1999). Soil moisture  
90 controls the partitioning of the available energy into latent and sensible heat flux and  
91 conditions the amount of surface runoff. By controlling evapotranspiration, it is linking the  
92 energy, water and carbon fluxes (Koster et al., 2004; Dirmeyer et al., 2006; Seneviratne and  
93 Stöckli, 2008). Seneviratne et al. (2006) stated that a northward shift of climatic regimes in  
94 Europe due to climate change will result in a new transitional climate zone between dry and  
95 wet climates with strong land–atmosphere coupling in central and eastern Europe. They  
96 specifically highlight the importance of soil-moisture–temperature feedbacks (in addition to  
97 soil-moisture–precipitation feedbacks) for future climate changes over this region. A  
98 comprehensive review on soil moisture feedbacks is given by Seneviratne et al. (2010).

99 Largely, soil moisture feedbacks to the atmosphere are confined to regions where the  
100 evapotranspiration is moisture-limited. These are regions where the soil moisture is in the  
101 transitional regime between the permanent wilting point (soil moisture content below which  
102 the plants can not extract water from the soil by transpiration as the suction forces of the soil  
103 are larger than the transpiration forces of the plants) and the critical soil moisture  $W_{crit}$  above  
104 which plants transpire at the potential rate imposed by the atmospheric conditions, i.e. the  
105 potential evapotranspiration (see, e.g., Fig. 5 in Seneviratne et al., 2010). In this respect, the  
106 high-latitudes are usually excluded from those regions as they are considered to be  
107 predominantly energy-limited (Teuling et al., 2009), and where the coupling between soil  
108 moisture and the atmosphere does not play a role (Koster et al., 2004, 2006).

109 Note that in previous studies where an ESM's land surface model (LSM) was equipped with  
110 cold region soil processes, effects of resulting model improvements usually have not been  
111 directly considered in a coupled atmosphere-land context. Either simulated changes were only  
112 considered in the LSM standalone mode (e.g. Ekici et al., 2014, 2015; Lawrence and Slater,  
113 2005; Gouttevin et al., 2012; Slater et al., 1998), or changes between different LSM version  
114 were not limited to cold region processes alone (Cox et al., 1999). Only Takata and Kimoto  
115 (2000) conducted a kind of precursor to our study who used a very coarse resolution  
116 atmospheric GCM (600 km resolution), but they neither used large-scale observations to  
117 evaluate the results of their study nor specifically addressed land-atmosphere feedbacks. Thus,  
118 soil moisture feedbacks to the atmosphere related to cold region soil processes have generally  
119 been neglected so far.

120 In the present study, we show that the implementation of cold region soil processes into the  
121 ESM of the Max Planck Institute for Meteorology, MPI-ESM, has a pronounced impact on  
122 the simulated terrestrial climate over the northern high latitudes, and that this is mainly related  
123 to a positive soil moisture-precipitation feedback. Section 2 introduces the used ESM version  
124 and the setup of the associated simulations, Section 3 discusses the main results over several  
125 high latitude river catchments, followed by a summary and conclusions in Section 4.

## 126 **2 Model, data and methods**

### 127 **2.1 Model description**

128 In this study, the atmosphere and land components of the ESM of the Max Planck Institute for  
129 Meteorology (MPI-M), MPI-ESM 1.1, are utilized that consist of the atmospheric GCM  
130 ECHAM6.3 (Stevens et al., 2013) and its land surface scheme JSBACH 3.0 (Raddatz et al.,  
131 2007, Brovkin et al., 2009). Both models have undergone several further developments since

132 the version (ECHAM6.1/JSBACH 2.0) used for the Coupled Model Intercomparison Project  
133 5 (CMIP5; Taylor et al., 2012). Several bug fixes in the ECHAM physical parameterizations  
134 led to energy conservation in the total parameterized physics and a re-calibration of the cloud  
135 processes resulted in a medium range climate sensitivity of about 3 K. JSBACH 3.0  
136 comprises several bug fixes, a new soil carbon model (Goll et al., 2015) and a five layer soil  
137 hydrology scheme (Hagemann and Stacke, 2015) replaced the previous bucket scheme. These  
138 five layers correspond directly to the structure used for soil temperatures and they are defined  
139 with increasing thickness (0.065, 0.254, 0.913, 2.902, and 5.7 m) down to a lower boundary at  
140 almost 10 m depth. In addition, a permafrost-ready version of JSBACH is considered  
141 (JSBACH-PF) in which physical processes relevant at high latitude land regions have been  
142 implemented by Ekici et al. (2014). Most importantly, these processes comprise the freezing  
143 and thawing of soil moisture. Consequently, the latent heat of fusion dampens the amplitude  
144 of soil temperature, infiltration is decreased when the uppermost soil layer is frozen, soil  
145 moisture is bound in solid phase when frozen, and, hence, cannot be transported vertically or  
146 horizontally. Dynamic soil thermal properties now depend on soil texture as well as on soil  
147 water and ice contents. Dynamic soil hydraulic properties that depend on soil texture and soil  
148 water content may decrease when soil moisture freezes (such as, e.g., the hydraulic  
149 conductivity). Moreover a snow scheme has been implemented in which snow can develop in  
150 up to five layers while the current scheme only represents up to two layers. In the original  
151 snow scheme, the snow is thermally growing down inside the soil, i.e. the snow cover  
152 becomes part of the soil temperature layers so that soil temperatures are mixed with snow  
153 temperatures. In the new scheme, snow is accumulated on top of the soil using snow thermal  
154 properties. Further, a homogeneous organic top layer is added with a constant depth and  
155 specific thermal and hydraulic properties. Note that in the following the term soil moisture  
156 generally refers to the liquid soil moisture if not mentioned otherwise. In this respect, total

157 soil moisture refers to the sum of liquid and frozen soil moisture.

## 158 **2.2 Experimental setup**

159 Two ECHAM6.3/JSBACH simulations were conducted at T63 horizontal resolution (about  
160 200 km) with 47 vertical layers in the atmosphere. They were forced by observed sea surface  
161 temperature (SST) and sea ice from the AMIP2 (Atmospheric Model Intercomparison Project  
162 2) dataset during 1970-2009 (Taylor et al., 2000). 1970-1988 are regarded as spin-up  
163 phase, only the period 1989-2009 is considered for the analyses. The two simulations are:

- 164 • ECH6-REF: Simulation with the standard version of JSBACH 3.0 with a fixed  
165 vegetation distribution and using a separate upper layer reservoir for bare soil  
166 evaporation as described in Hagemann and Stacke (2015). Note that the latter is  
167 switched off by default in JSBACH 3.0 to achieve a better performance of simulated  
168 primary productivity, which is not of interest in the present study.
- 169 • ECH6-PF: As ECH6-REF, but using JSBACH-PF.

170 Note that both simulations used initial values of soil moisture, soil temperature and snowpack  
171 that were obtained from an offline-simulation (land only) using JSBACH (as in ECH6-REF)  
172 forced with WFDEI data (Weedon et al., 2014).

## 173 **2.3 Calculation of internal model climate variability**

174 The internal climate variability of ECHAM6/JSBACH with respect to 20-year mean values  
175 has been estimated from results of three 20-year, 5-member ensembles, in which the  
176 ensembles used different land-atmosphere coupling setups (deVrese et al., 2016). Within each  
177 ensemble, the model setup is identical but the simulations were started using slightly differing  
178 initial conditions. Following the approach of Hagemann et al. (2009), we first calculated the



179 standard deviation of 20-year means for each ensemble, and then the spread for each model  
180 grid box is defined as the maximum of the three ensemble standard deviations. This spread is  
181 then used as an estimate of the model's internal climate variability. Thus, if simulated  
182 differences between ECH6-PF and ECH6-REF are larger than this spread, they are considered  
183 as robust and directly related to the introduction of cold region soil processes into JSBACH.

#### 184 **2.4 Observational data**

185 We use climatological observed river discharges from the station network of the Global  
186 Runoff Data Centre (Dümenil Gates et al., 2000). Near surface air (2m) temperature and  
187 precipitation are taken from the recent global WATCH dataset of hydrological forcing data  
188 (WFDEI; Weedon et al., 2014). The WFDEI combine the daily statistics of the Interim re-  
189 analysis of the European Centre for Medium-Range Weather Forecasts (ERA-Interim; Dee et  
190 al., 2011) with the monthly mean observed characteristics of temperature from the Climate  
191 Research Unit dataset TS2.1 (CRU; Mitchell and Jones, 2005) and precipitation from the  
192 Global Precipitation Climatology Centre full dataset version 4 (GPCC; Fuchs et al., 2007).  
193 For the latter, a gauge-undercatch correction following Adam and Lettenmaier (2003) was  
194 used, which takes into account the systematic underestimation of precipitation measurements  
195 that have an error of up to 10-50% (see, e.g. Rudolf and Rubel, 2005).

196 For an estimate of observed evapotranspiration (ET), we are using data from the LandFlux-  
197 EVAL dataset. This new product was generated to compile multi-year global merged  
198 benchmark synthesis products based on the analyses of existing land evapotranspiration  
199 datasets (monthly time scale, time periods 1989-1995 and 1989-2005). The calculation and  
200 analyses of the products are described in Mueller et al. (2013). In our study we are using the  
201 diagnostic products available for the period 1989-2005 that are based on various observations,  
202 i.e. from remote sensing, diagnostic estimates (atmospheric water-balance estimates) and

203 ground observations (flux measurements). Here, we considered the mean, minimum and  
204 maximum of the respective diagnostic ensemble.

205 Surface solar irradiance (SSI; 2000-2010) is taken from the Clouds and Earth Radiation  
206 Energy System (CERES; Kato et al., 2013) that provides surface solar radiation fluxes at  
207 global scale derived from measurements onboard of the EOS Terra and Aqua satellites (Loeb  
208 et al., 2012). We used surface albedo data from MODIS (MCD43C3, ver5; 2000-2011;  
209 Cescatti et al., 2012), CERES (2000-2010) and the GlobAlbedo project (1998-2011; Muller et  
210 al., 2012) of the European Space Agency (ESA). With regard to the accumulated snowpack,  
211 we compared model data to snow water equivalent data from the ESA GlobSnow project  
212 (Takala et al., 2011), NASA's Modern-Era Retrospective Analysis for Research and  
213 Applications (MERRA; 1979-2013; Rienecker et al., 2011) and the snow data climatology  
214 (SDC) of Foster and Davy (1988).

### 215 **3 Results**

216 The simulations ECH6-REF and ECH6-PF are evaluated over the northern high latitudes  
217 analogously to how the evaluation of surface water and energy fluxes of the CMIP5 version of  
218 MPI-ESM was conducted by Hagemann et al. (2013b). The main differences in precipitation  
219 and 2m temperature between both simulations occur in the boreal summer. In ECH6-PF,  
220 precipitation is generally reduced compared to ECH6-REF over the northern high latitudes  
221 (Fig. 1). On the one hand, this leads to a general reduction of the wet bias compared to  
222 WFDEI data over the more continental areas north of about 60°N, especially over Canada and  
223 Russia. On the other hand, it enhances the dry bias over the adjacent mid-latitudes. Note that  
224 this summer dry bias of MPI-ESM 1.1 over mid-latitudes is more pronounced and wide-  
225 spread than in the CMIP5 version of MPI-ESM (cf. Fig. 4, middle row, in Hagemann et al.,

226 2013b), which is likely associated with bug-fixes or the re-calibration of cloud processes in  
227 ECHAM6.3 (cf. Sect. 2.1). The same is also the case for northern hemisphere summer warm  
228 biases in ECH6-REF (Fig. 2). These warm biases are enhanced in ECH6-PF. This  
229 enhancement is partly related to the fact that the reduced precipitation is accompanied by a  
230 reduced cloud cover, and, hence an increased incoming solar radiation at the land surface  
231 (Fig. 3). Compared to CERES data, the low bias in SSI over the high latitudes is largely  
232 removed while the overestimation over the mid-latitudes is slightly increased. The reason for  
233 the warmer air temperatures can partly be found in a decreased evapotranspiration (ET) when  
234 permafrost relevant physical soil processes are switched on. A detailed analysis of their  
235 effects was carried out to elucidate the specific influence of these processes and is shown for  
236 two large example catchments (Fig. 4). 1) The Arctic catchment is represented by the six  
237 largest rivers flowing into the Arctic Ocean: Kolyma, Lena, Mackenzie, Northern Dvina, Ob  
238 and Yenisei. The associated catchments comprise a large fraction of permafrost covered areas.  
239 2) The Baltic Sea catchment includes only a low amount of permafrost covered areas but soil  
240 moisture freezing still plays a role over large parts of the catchment during the winter.

#### 241 *Arctic River catchments*

242 ECH6-PF simulates the discharge of the six largest Arctic rivers more reliably than ECH6-  
243 REF, especially with regard to timing and size of the snow melt induced discharge peak in  
244 spring (Fig. 5a). This is largely related to the fact that in ECH6-PF, a major part of the snow  
245 melt turns into surface runoff as it cannot infiltrate into the ground when this is still frozen in  
246 the beginning of spring. This is opposite to ECH6-REF where larger parts of the snow melt  
247 are infiltrating into the soil due to the missing freezing processes such that the observed  
248 discharge peak is largely underestimated.

249 Consistent with Fig. 1, the large wet bias in the summer precipitation of ECH6-REF is

250 strongly reduced in ECH6-PF (Fig. 5c). This reduction in summer precipitation is  
251 accompanied by a reduction in summer evapotranspiration (Fig. 6a) that is now much closer  
252 to the mean of diagnostic estimates from the LandFlux dataset, while it is likely overestimated  
253 in ECH6-REF as the simulated evapotranspiration is close to the upper limit of the LandFlux  
254 diagnostic estimates. This ET reduction in ECH6-PF is directly related to a completely  
255 changed seasonal cycle of liquid relative soil moisture (actual soil moisture divided by the  
256 maximum soil water holding capacity) in the root zone (Fig. 6c). In ECH6-REF, the soil is  
257 very wet throughout the whole year with somewhat lower values in summer that are related to  
258 the summer ET. In ECH6-PF, the soil is rather dry in winter as larger parts of the total soil  
259 moisture are frozen (Fig. 7), and, hence, not accessible for ET. With infiltration of snowmelt  
260 in the spring when the soil water of the upper layer has thawed, the soil moisture is increasing  
261 and reaches its maximum in summer. The total amount of liquid soil moisture in ECH6-PF is  
262 much lower than in ECH6-REF. On the one hand large parts of the soil are frozen in winter  
263 and adjacent months (Fig. 7), and on the other hand this is related to the much lower  
264 infiltration in spring, so that less soil moisture is available throughout the whole year. In the  
265 autumn and winter, the amount of total soil moisture is somewhat increasing (Fig. 6c) as due  
266 to freezing, it is locally bound and can neither flow off laterally nor evaporate. If compared to  
267 the model's internal climate variability (Fig. 8) we note that the differences between ECH6-  
268 PF and ECH6-REF are robust for ET and precipitation from April-October and April-August,  
269 respectively.

270 The decreased ET during warm months, however, brings about less evaporative cooling of the  
271 land surface and a reduced upward moisture flux into the atmosphere that in turn seems to  
272 reduce cloud cover, and, hence SSI is increased in ECH6-PF (Fig. 9c, see also Fig. 3). Both of  
273 these effects result in a further increase of the summer warm bias in 2m air temperature (Fig.  
274 9a, see also Fig. 2).

275 The surface albedo is rather similar in both experiments (Fig. 10a) but shows some distinct  
276 biases if compared to various observational datasets. During the winter JSBACH seems to  
277 overestimate the mainly snow-related albedo, indicating that it may have difficulties to  
278 adequately represent snow-masking effect of boreal forests [Note that a version of MODIS  
279 albedo data was used where low quality data over the very high northern latitudes were  
280 filtered out in the boreal winter due to too low available radiation (A. Löw, pers. comm.,  
281 2016). Due to these missing data over mainly snow covered areas, MODIS albedo averaged  
282 over the six largest Arctic rivers is biased low in the winter]. During the summer, there is a  
283 larger uncertainty in the observations. While the simulated albedo is close to MODIS and  
284 CERES data, it is lower than GlobAlbedo data. As a too low albedo would lead to a warm  
285 bias, this might indicate a better reliability of the GlobAlbedo data for this region in summer.  
286 Note that a sensitivity test where surface albedo was increased by 0.05 north of 60°N led to a  
287 reduction of the warm bias by about 1-2 K (not shown). As already indicated by the surface  
288 albedo, the simulated snow cover does not significantly differ between the experiments, either  
289 (Fig. 10c). It is lower than various observational estimates, which should impose a low albedo  
290 bias in winter. As this bias is in the opposite direction, it can be concluded that the low snow  
291 pack is compensating part of the snow masking problem mentioned above.

### 292 *Baltic Sea catchment*

293 A similar effect of the frozen ground is found over the Baltic Sea catchment, although this is  
294 less strong than for the Arctic rivers. The frozen ground leads to an enhanced snow melt  
295 runoff in spring (Fig. 5b) and a less strong replenishment of the ground by water during the  
296 winter as it is the case for ECH6-REF (Fig. 6d). Consequently the average level of liquid soil  
297 moisture is lower in ECH6-PF compared to ECH6-REF. This leads to more infiltration of  
298 water and less drainage, and hence, less runoff in the summer, which in turns leads to an

299 improved simulation of discharge (Fig. 5b). The impact on the atmosphere is much less  
300 pronounced than for the Arctic rivers. On one hand there is less frozen ground in the Baltic  
301 Sea catchment (Fig. 7), on the other hand the average soil moisture content is larger than for  
302 the Arctic rivers (Fig. 6d). In ECH6-REF, the soil moisture is generally above  $W_{crit}$  (c.f. Sect.  
303 1) in the Baltic Sea catchment so that ET is largely energy limited and mostly occurring at its  
304 potential rate. Even though the ECH6-PF soil moisture is lower, it is generally still close to  
305  $W_{crit}$  so that ET is only slightly reduced, especially in the second half of the year (Fig. 6b).  
306 Precipitation is also somewhat reduced (Fig. 5d) but this seems to be mostly related to the  
307 internal climate variability except for September and October when a somewhat stronger and  
308 robust reduction in ET leads to a robust precipitation decrease (Fig. 8).

#### 309 **4 Discussion and conclusions**

310 The results described in the previous section show that soil freezing and thawing processes  
311 enable the positive soil moisture-precipitation feedback (e.g. Dirmeyer et al., 2006;  
312 Seneviratne et al., 2010) over large parts of northern mid- and high latitudes during the boreal  
313 summer. The chain of processes leading to and influencing this feedback is sketched in Fig.  
314 11. The frozen soil during the cold season (late autumn to early spring) leads to less  
315 infiltration of rainfall and snowmelt during this season, and, hence, to more surface runoff  
316 especially during the snowmelt period. On one hand this leads to a large improvement in  
317 simulated discharge, mainly due to the improved snowmelt peak. This improved discharge  
318 due to the representation of frozen ground has been also reported for other models (Beer et al.,  
319 2006, 2007; Ekici et al., 2014; Gouttevin et al., 2012). On the other hand, this leads to a  
320 decrease of soil moisture. This spring soil moisture deficit from the increased discharge  
321 extends into the boreal summer due to the soil moisture memory (e.g. Koster and Suarez 2001,  
322 Orth and Seneviratne 2012), when it actually causes more infiltration and less runoff, and,

323 hence, less discharge. The latter strongly improves the simulated discharge in the Baltic Sea  
324 catchment from summer to early winter. The decreased soil moisture leads to a reduced ET in  
325 regions where the soil moisture is in the transitional regime. Here, there is less recycling of  
326 moisture into the atmosphere, and the lower atmospheric moisture causes a reduction of  
327 precipitation that in turn leads to a further reduction of soil moisture.

328 Our new finding of the importance of the positive soil moisture-precipitation feedback in  
329 northern high latitudes has been supported by correlations between soil moisture and  
330 precipitation using monthly values from 1989-2009. While there are higher correlations  
331 between soil moisture and precipitation in the mid-latitudes for ECH6-REF (Fig. 12a), the  
332 high latitudes are mostly characterized by rather low correlations using the reference version  
333 of JSBACH. Figure 13b and c show that the correlation between soil moisture and  
334 precipitation is strongly increased in ECH6-PF over large parts of the northern high latitudes,  
335 especially over North America and eastern Siberia. This confirms an increased coupling of  
336 soil moisture and precipitation, and, hence, also indicates that the soil moisture-precipitation  
337 feedback is highly enabled in these areas. This positive soil moisture-precipitation feedback  
338 improves the simulated hydrological cycle, especially over the Arctic rivers where the wet  
339 biases in summer precipitation and ET are reduced. Less ET, and, hence, less evaporative  
340 cooling cause an increase in summer 2m air temperatures. This, in combination with more  
341 incoming surface solar radiation due to fewer clouds, increases and extends the existing  
342 summer warm bias of MPI-ESM north of about 50°N. Since air temperature is a main driver  
343 of soil freezing and thawing processes, there are more indirect interactions between energy  
344 and water balances which call for even more advanced factorial model experiments in the  
345 future.

346 Changes in the simulated hydrological cycle induced by the utilization of the improved soil

347 scheme are mostly confined to areas where freezing and thawing of water play a role. To  
348 illustrate this, Fig. 13 shows the number of months where in the climatological average of  
349 1989-2009, the upper soil layer is below 0°C in ECH6-PF. Changes in precipitation (Fig. 1)  
350 and surface solar irradiance (Fig. 3), indicating changes in cloud cover, are mostly located in  
351 regions where the upper layer is frozen for at least three months within the climatological  
352 average. Changes outside of regions with soil frost may be imposed by changed atmospheric  
353 humidity and heat transport from soil frost affected regions on the one hand. On the other  
354 hand, Ekici et al. (2014) also introduced a permanent, static organic top layer as part of the  
355 new JSBACH-PF soil scheme. If switched on, as in the current ECH6-PF simulation, it is  
356 considered globally uniform, thus introducing a soil isolating effect also outside permafrost  
357 regions. As a consequence, the partitioning of the surface heat balance is altered during snow-  
358 free months towards a decreased ground heat flux, which needs to be compensated for by the  
359 turbulent heat fluxes, in particular by the sensible heat flux. This in turn contributes to the  
360 warming of the 2m air temperature which can be seen also in areas without any soil frost (Fig.  
361 2). Even though the uniform organic insulation layer was implemented globally, Fig. 12  
362 shows that the correlation between soil moisture and precipitation advances strongly in  
363 northern high latitudes only while this correlation has nearly not changed in the temperate  
364 zone and in particular in drought-dominated areas in south-east Europe or mid-west USA.  
365 Note that currently, the land surface scheme has been further advanced by a mechanistic  
366 model of mosses and lichens dynamics (Porada et al., 2016) which will replace the actual  
367 static organic top layer for soil insulation. This will enable a more realistic representation of  
368 the temporal and spatial variation of the soil insulation.

369 A positive soil moisture-precipitation feedback has not been pointed out for the northern high  
370 latitudes so far, even though in their coarse resolution GCM study, Takata and Kimoto (2000)  
371 found similar impacts to those shown in Fig. 11 induced by soil water freezing. Previously,



372 the northern high latitudes have generally been considered as energy-limited regimes where  
373 land-atmosphere coupling due to soil moisture does not play a role (e.g. Teuling et al., 2009).  
374 But this principal feedback loop has been found for drier regions where the soil moisture is  
375 generally in the transitional regime and land-atmosphere coupling plays a role. Koster et al.  
376 (2004) considered the strength of coupling between soil moisture and precipitation in an  
377 ensemble of atmospheric GCMs. The resulting map is very similar to the map regarding the  
378 strength of coupling between soil moisture and temperature in the same GCMs (Koster et al.,  
379 2006). This suggests that in these models, the same process controls both couplings, namely  
380 the ET sensitivity to soil moisture that leads to a positive feedback (Seneviratne et al., 2010).  
381 But on the one hand it can be assumed that many models participating in those earlier studies  
382 did not include the freezing and thawing of soil water. Thus, our reference simulation ECH6-  
383 REF is in line with results reported in the literature, generally not showing a strong coupling  
384 between precipitation and soil moisture in permafrost regions, such as indicated by the rather  
385 low correlation values in Fig. 12a. Only the ECH6-PF simulation using advanced soil physics  
386 shows that such strong coupling indeed is present (Fig. 12b). On the other hand, only annual  
387 mean diagnostics were considered in some of those earlier studies (e.g. Teuling et al., 2009).  
388 In other land-atmosphere coupling studies, that, e.g., followed the GLACE protocol such as  
389 Koster et al. (2004), prescribed soil moisture conditions were used that were similar to the  
390 average soil moisture climatology. Here, it seems that the differences between the simulations  
391 with free and prescribed soil moisture in GLACE type simulations may be not large enough to  
392 reveal a large-scale feedback over the high latitudes. This may only be possible by an  
393 experimental design where more pronounced summer soil moisture changes are introduced.  
394 Note that in the present study, these pronounced changes were introduced not due to an  
395 artificial design, but they were caused by the implementation of previously missing frozen  
396 soil physics into the model. Our study has shown that spring moisture deficits can lead to soil

397 moisture conditions during the boreal summer that allow for an advanced land-atmosphere  
398 coupling and a positive soil moisture-precipitation feedback over the northern high latitudes.

399 Even though our results are obtained with a modelling study, their physical consistency  
400 suggests that cold region soil processes, especially freezing and thawing of soil water, may  
401 lead to a positive soil moisture precipitation feedback during the summer in reality, too. A  
402 prerequisite for the occurrence of a soil moisture precipitation feedback is that soil moisture is  
403 in the transitional regime. Thus, the strength of the feedback depends on the wetness of the  
404 soil and, hence, is likely model dependent. Models with wetter/drier soils over the considered  
405 regions may simulate a weaker/stronger feedback.

406 Several modelling studies pointed out that there are not only positive feedback loops between  
407 soil moisture and precipitation but also negative ones that, under specific conditions, such as  
408 convective instability and/or cloud formation, may be stronger over dry soils (e.g.  
409 Hohenegger et al., 2009; Froidevaux et al., 2014). However, to date, the latter results appear  
410 mostly confined to single-column, cloud-resolving, and some high-resolution regional climate  
411 simulations (Seneviratne et al., 2010) and may also depend on the choice of the convective  
412 parameterisations (e.g. Giorgi et al., 1996). Guillod et al. (2015) noted that precipitation  
413 events tend to be located over drier patches, but they generally need to be surrounded by wet  
414 conditions; positive temporal soil moisture-precipitation relationships are thus driven by  
415 large-scale soil moisture. Thus, negative feedbacks seem to have more an impact on high  
416 resolution and thus on the local scale (Ho-Hagemann et al., 2015), where the effects of land  
417 surface heterogeneity for the inferred feedbacks also need to be taken into account (Chen and  
418 Avissar, 1994; Pielke et al., 1998; Taylor et al., 2013). Consequently most GCMs may not be  
419 able to represent negative feedbacks between soil moisture and precipitation via ET. As in the  
420 present study, we considered the effect of large-scale soil moisture changes due to soil

421 freezing processes, the identification of potential negative feedbacks on the local scale is  
422 beyond the scope of the present study.

423 In MPI-ESM, an unwelcome effect of implementing cold region soil processes is the increase  
424 of the existing warm bias over the high latitudes during summer. In order to estimate the  
425 contribution of biases in SSI and surface albedo to this warm bias, we calculated an upper  
426 limit for the temperature change that may be imposed by a radiation difference in the related  
427 energy flux into the ground [ $SSI \times (1 - \text{albedo})$ ]. For this estimation we assume that the  
428 surface temperature is adjusting in a way that this radiation difference is compensated by  
429 thermal radiation following the Stefan Boltzmann law. Here, any change in the turbulent  
430 surface heat fluxes is neglected so that the resulting temperature change is an upper limit for  
431 the temperature bias that might be explained by a radiation bias.

432 Considering the mean summer biases over the six largest Arctic rivers (Table 1) indicates that  
433 a part of the warm bias may be attributed to the overestimation in SSI. For ECH6-PF (ECH6-  
434 REF), the SSI bias may cause a warm bias of up to 2.9 K (0.9 K). The surface albedo may  
435 contribute another 0.7 K (0.8 K) to the warm bias if compared to GlobAlbedo data but this is  
436 a rather vague estimation due to the large uncertainty on surface albedo observations (see Fig.  
437 10). Nevertheless biases in both of these variables cannot explain the full bias of 5 K (2.1 K)  
438 in 2m temperature. Further contributions to this warm bias might be related to a too weak  
439 vertical mixing of heat within the boundary layer or too much advection of warm air. The  
440 latter may also influence the recycling ratio of water within and outside regions of soil frost.  
441 A deeper investigation of this is beyond the scope of the present study and should be dealt  
442 with in future model improvements.

443 We have shown that soil physical processes such as thawing and freezing have an impact on  
444 the regional climate over the high latitude permafrost areas. Flato et al. (2013) reported that

445 CMIP5 GCMs tend to overestimate precipitation over northern high latitudes except for  
446 Europe and western Siberia. As many of these GCMs are still missing basic cold region  
447 processes, a missing interaction between soil moisture and precipitation in those GCMs is  
448 likely to contribute to this wet bias. An adequate implementation of physical soil processes  
449 into an ESM is only the first necessary step to yield an adequate representation of land-  
450 atmosphere interactions over the high latitudes. This also includes the incorporation of  
451 wetland dynamics, which will be the next step in the JSBACH development with regard to  
452 high latitudes, thereby following an approach of Stacke and Hagemann (2012). In addition, a  
453 reliable hydrological scheme for permafrost regions will allow investigations of related  
454 climate-carbon cycle feedback mechanisms (McGuire et al., 2006; Beer, 2008; Heimann and  
455 Reichstein, 2008).

456 Our findings demonstrate that soil freezing and thawing induce a much stronger coupling of  
457 land and atmosphere in northern high latitudes than previously thought. The additional  
458 importance of the positive soil moisture precipitation feedback in high latitudes will have a  
459 strong impact on future climate projections in addition to other biophysical (e.g. albedo) or  
460 biogeochemical (e.g. climate-carbon cycle) feedback mechanisms. Therefore, the findings of  
461 this study additionally highlight the importance of permafrost ecosystem functions in relation  
462 to climate.

### 463 **Acknowledgments**

464 The authors acknowledge the financial support of T. Blome by the European Union FP7-ENV  
465 project PAGE21 under contract number GA282700. S. Hagemann is supported by funding  
466 from the European Union within the Horizon 2020 project CRESCENDO (grant no. 641816).

467

468 **References**

- 469 ACIA: Arctic Climate Impact Assessment, Cambridge University Press, 1042p.,  
470 <http://www.acia.uaf.edu>, 2005.
- 471 Adam, J. C., and, Lettenmaier, D. P.: Adjustment of global gridded precipitation for  
472 systematic bias, *J. Geophys. Res.*, 108, D9, 4257, doi:10.1029/2002JD002499, 2003.
- 473 Beer, C.: Soil science: The Arctic carbon count, *Nature Geoscience*, 1, 569-570,  
474 doi:10.1038/ngeo292, 2008.
- 475 Beer, C., Lucht, W., Schmullius, C., and Shvidenko, A.: Small net carbon dioxide uptake by  
476 Russian forests during 1981–1999, *Geophys. Res. Lett.*, 33, L15403,  
477 doi:10.1029/2006GL026919, 2006.
- 478 Beer, C., Lucht, W., Gerten, D., Thonicke, K., and Schmullius, C.: Effects of soil freezing and  
479 thawing on vegetation carbon density in Siberia: A modeling analysis with the Lund-  
480 Potsdam-Jena Dynamic Global Vegetation Model (LPJ-DGVM), *Global Biogeochem.*  
481 *Cyc.*, 21, GB1012, doi:10.1029/2006GB002760, 2007.
- 482 Brovkin, V., Raddatz, T., Reick, C. H., Claussen, M., and Gayler, V.: Global biogeophysical  
483 interactions between forest and climate, *Geophys. Res. Letters*, 36, L07 405,  
484 doi:10.1029/2009GL037543, 2009.
- 485 Brown, J., Ferrians Jr., O. J., Heginbottom, J. A., and Melnikov, E. S. (eds.): Circum-Arctic  
486 map of permafrost and ground-ice conditions, Washington, DC: U.S. Geological Survey  
487 in Cooperation with the Circum-Pacific Council for Energy and Mineral Resources.  
488 Circum-Pacific Map Series CP-45, scale 1:10,000,000, 1997.
- 489 Cescatti, A., Marcolla, B., Santhana Vannan, S. K., Pan, J. Y., Román, M. O., Yang, X.,  
490 Ciais, P., Cook, R. B., Law, B. E., Matteucci, G., Migliavacca, M., Moors, E.,

491 Richardson, A. D., Seufert, G., and Schaaf, C.B.: Intercomparison of MODIS albedo  
492 retrievals and in situ measurements across the global FLUXNET network, *Rem. Sens.*  
493 *Environ.*, 121, 323-334, 2012.

494 Chen, F., and Avissar, R.: Impact of land-surface moisture variability on local shallow  
495 convective cumulus and precipitation in large-scale models, *J. Appl. Meteorol.*, 33 (12),  
496 1382–1401, 1994.

497 Cox, P., Betts, R., Bunton, C., Essery, R., Rowntree, P., and Smith, J.: The impact of new  
498 land surface physics on the GCM simulation. of climate and climate sensitivity, *Climate*  
499 *Dyn.*, 15, 183–203, doi:10.1007/s003820050276, 1999.

500 de Vrese, P., and Hagemann, S.: Explicit representation of spatial sub-grid scale heterogeneity  
501 in an ESM, *J. Hydrometeorol.*, 17, 1357-1371, doi:10.1175/JHM-D-15-0080.1., 2016.

502 Dee, D. P., Uppala, S. M., Simmons, A. J., Berrisford, P., Poli, P., Kobayashi, S., Andrae, U.,  
503 Balmaseda, M. A., Balsamo, G., Bauer, P., Bechtold, P., Beljaars, A. C. M., van de Berg,  
504 L., Bidlot, J., Bormann, N., Delsol, C., Dragani, R., Fuentes, M., Geer, A. J., Haimberger,  
505 L., Healy, S. B., Hersbach, H., Hólm, E. V., Isaksen, L., Kållberg, P., Köhler, M.,  
506 Matricardi, M., McNally, A. P., Monge-Sanz, B. M., Morcrette, J.-J., Park, B.-K.,  
507 Peubey, C., de Rosnay, P., Tavolato, C., Thépaut, J.-N., and Vitart, F.: The ERA-interim  
508 reanalysis: configuration and performance of the data assimilation system, *Q. J. Roy.*  
509 *Meteorol. Soc.*, 137, 553–597, doi:10.1002/qj.828, 2011.

510 Dirmeyer, P., Koster, R., and Guo, Z. A. D.: Do global models properly represent the  
511 feedback between land and atmosphere?, *J. Hydrometeorol.*, 7, 1177–1198, 2006.

512 Dümenil Gates, L., Hagemann, S., and Golz, C.: Observed historical discharge data from  
513 major rivers for climate model validation, Max Planck Institute for Meteor. Rep., 307  
514 [available from MPI for Meteorology, Bundesstr. 53, 20146 Hamburg, Germany], 2000.

515 Ekici, A., Beer, C., Hagemann, S., Boike, J., Langer, M., and Hauck, C.: Simulating high  
516 latitude permafrost regions by the JSBACH terrestrial ecosystem model, *Geosci. Model*  
517 *Dev.*, 7, 631-647, doi:10.5194/gmd-7-631-2014, 2014.

518 Ekici, A., Chadburn, S., Chaudhary, N., Hajdu, L. H., Marmy, A., Peng, S., Boike, J., Burke,  
519 E., Friend, A. D., Hauck, C., Krinner, G., Langer, M., Miller, P. A., and Beer, C.: Site-  
520 level model intercomparison of high latitude and high altitude soil thermal dynamics in  
521 tundra and barren landscapes, *The Cryosphere*, 9, 1343-1361, doi:10.5194/tc-9-1343-  
522 2015, 2015.

523 Flato, G., Marotzke, J., Abiodun, B., Braconnot, P., Chou, S. C., Collins, W., Cox, P.,  
524 Driouech, F., Emori, S., Eyring, V., Forest, C., Gleckler, P., Guilyardi, E., Jakob, C.,  
525 Kattsov, V., Reason, C., and Rummukainen, M.: Evaluation of Climate Models. In:  
526 *Climate Change 2013: The Physical Science Basis, Contribution of Working Group I to*  
527 *the Fifth Assessment Report of the Intergovernmental Panel on Climate Change* [Stocker,  
528 T.F., Qin, D., Plattner, G.-K., Tignor, M., Allen, S. K., Boschung, J., Nauels, A., Xia, Y.,  
529 Bex, V., and Midgley, P. M. (eds.)]. Cambridge University Press, Cambridge, United  
530 Kingdom and New York, NY, USA, 2013.

531 Foster, D. J., and Davy, R.D.: Global snow data climatology, USAFETAC/TN-88/006, Scott  
532 Air Force Base III, 1988.

533 French, H. M.: Editorial, *Permafrost Periglac. Process*, 1, 1, doi: 10.1002/ppp.3430010102,  
534 1990.

535 Froidevaux, P., Schlemmer, L., Schmidli, J., Langhans, W., and Schär, C.: Influence of  
536 background wind on the local soil moisture-precipitation feedback, *J. Atmos. Sci.*, 71,  
537 782-799, 2014.

538 Fuchs, T., Schneider, U., and Rudolf, B.: Global Precipitation Analysis Products of the

539 GPCC, Global Precipitation Climatology Centre (GPCC). Deutscher Wetterdienst,  
540 Offenbach, Germany, 2007.

541 Giorgi, F., Mearns, L.O., Shields, C., and Mayer, L.: A regional model study of the  
542 importance of local versus remote controls of the 1988 drought and the 1993 flood over  
543 the central United States, *J. Climate*, 9, 1150–1162, 1996.

544 Goll, D. S., Brovkin, V., Liski, J., Raddatz, T., Thum, T., and Todd-Brown, K. E. O.: Strong  
545 dependence of CO<sub>2</sub> emissions from anthropogenic land cover change on initial land cover  
546 and soil carbon parametrization, *Global Biogeochem. Cycles*, 29, 1511–1523,  
547 doi:10.1002/2014GB004988, 2015.

548 Gouttevin, I., Krinner, G., Ciais, P., Polcher, J., and Legout, C.: Multi-scale validation of a  
549 new soil freezing scheme for a land-surface model with physically-based hydrology, *The*  
550 *Cryosphere*, 6, 407-430, doi:10.5194/tc-6-407-2012, 2012.

551 Guillod, B. P., Orlowsky, B., Miralles, D. G., Teuling, A. J., and Seneviratne, S. I.:  
552 Reconciling spatial and temporal soil moisture effects on afternoon rainfall, *Nat.*  
553 *Commun.*, 6, 6443, doi: 10.1038/ncomms7443, 2015.

554 Hagemann, S., Göttel, H., Jacob, D., Lorenz, P., and Roeckner, E.: Improved regional scale  
555 processes reflected in projected hydrological changes over large European catchments,  
556 *Climate Dyn.*, 32, 767-781, doi: 10.1007/s00382-008-0403-9, 2009.

557 Hagemann, S., Blome, T., Saeed, F., and Stacke, T.: Perspectives in modelling climate-  
558 hydrology interactions, *Surveys in Geophys.*, 35, 739-764, ISSI special issue on  
559 Hydrological Cycle, doi:10.1007/s10712-013-9245-z, 2013a.

560 Hagemann, S., Loew, A., Andersson, A.: Combined evaluation of MPI-ESM land surface  
561 water and energy fluxes, *J. Adv. Model. Earth Syst.*, 5, doi:10.1029/2012MS000173,  
562 2013b.



563 Hagemann, S., and Stacke, T.: Impact of the soil hydrology scheme on simulated soil  
564 moisture memory, *Climate Dyn.*, 44, 1731-1750, doi:10.1007/s00382-014-2221-6, 2015.

565 Heimann, M., and Reichstein, M.: Terrestrial ecosystem carbon dynamics and climate  
566 feedbacks, *Nature*, 451, 289-292, 2008.

567 Ho-Hagemann, H. T. M., Rockel, B., and Hagemann, S.: On the role of soil moisture in the  
568 generation of heavy rainfall during the Oder flood event in July 1997, *Tellus A*, 67,  
569 28661, dx.doi.org/10.3402/tellusa.v67.28661, 2015.

570 Hohenegger, C., Brockhaus, P., Bretherton, C. S., and Schär, C.: The Soil Moisture–  
571 Precipitation Feedback in Simulations with Explicit and Parameterized Convection, *J.*  
572 *Climate*, 22, 5003–5020, 2009.

573 Hugelius, G., Strauss, J., Zubrzycki, S., Harden, J. W., Schuur, E. A. G., Ping, C.-L.,  
574 Schirrmeister, L., Grosse, G., Michaelson, G. J., Koven, C. D., O'Donnell, J. A.,  
575 Elberling, B., Mishra, U., Camill, P., Yu, Z., Palmtag, J., and Kuhry, P.: Estimated stocks  
576 of circumpolar permafrost carbon with quantified uncertainty ranges and identified data  
577 gaps, *Biogeosciences*, 11, 6573-6593, doi:10.5194/bg-11-6573-2014, 2014.

578 Kato, S., Loeb, N. G., Rose, F. G., Doelling, D. R., Rutan, D. A., Caldwell, T. E., Yu, L., and  
579 Weller, R. A.: Surface irradiances consistent with CERES-derived top-of-atmosphere  
580 shortwave and longwave irradiances, *J. Climate*, 26, 2719-2740, doi: 10.1175/JCLI-D-12-  
581 00436.1, 2013.

582 Koren, V., Schaake, J., Mitchell, K., Duan, O. Y., Chen, F., and Baker, J. M.: A  
583 parameterization of snowpack and frozen ground intended for NCEP weather and climate  
584 models, *J. Geophys. Res.*, 104, 19569–19585, 1999.

585 Koster, R. D., and Suarez, M. J.: Soil moisture memory in climate models. *J. Hydrometeorol.*,  
586 2, 558-570, 2001.

587 Koster, R. D., Dirmeyer, P. A., Guo, Z., Bonan, G., Chan, E., Cox, P., Gordon, C. T., Kanae,  
588 S., Kowalczyk, E., Lawrence, D., Liu, P., Lu, C. H., Malyshev, S., McAvaney, B.,  
589 Mitchell, K., Mocko, D., Oki, T., Oleson, K., Pitman, A., Sud, Y. C., Taylor, C. M.,  
590 Versegny, D., Vasic, R., Xue, Y., and Yamada, T.: Regions of strong coupling between  
591 soil moisture and precipitation, *Science*, 305, 1138–1140, 2004.

592 Koster R. D., Guo, Z., Dirmeyer, P. A., Bonan,, G., Chan, E., Cox, P., Davies, H., Gordon, C.  
593 T., Kanae, S., Kowalczyk, E., Lawrence, D., Liu, P., Lu, C. H., Malyshev, S., McAvaney,  
594 B., Mitchell, K., Mocko, D., Oki, T., Oleson, K. W., Pitman, A., Sud, Y. C., Taylor, C.  
595 M., Versegny, D., Vasic, R., Xue, Y., and Yamada, T.: GLACE: The Global Land-  
596 Atmosphere Coupling Experiment. Part I: Overview, *J. Hydrometeorol.*, 7, 590–610,  
597 2006.

598 Koven, C. D., Riley, W. J., and Stern, A.: Analysis of permafrost thermal dynamics and  
599 response to climate change in the CMIP5 Earth System Models, *J. Climate*, 26, 1877-  
600 1900, doi:10.1175/JCLI-D-12-00228.1, 2012.

601 Lawrence, D. M., and Slater, A. G.: A projection of severe near-surface permafrost  
602 degradation during the 21st century, *Geophys. Res. Lett.*, 32, L24401,  
603 doi:10.1029/2005GL025080, 2005.

604 Loeb, N. G., Kato, S., Su, W., Wong, T., Rose, F. G., Doelling, D. R., and Norris, J.:  
605 Advances in understanding top-of-atmosphere radiation variability from satellite  
606 observations, *Surveys in Geophysics*, doi: 10.1007/s10712-012-9175-1, 2012.

607 Luo, L. F., Robock, A., Vinnikov, K. Y., Schlosser, C. A., Slater, A. G., Boone, A., Braden,  
608 H., Cox, P., de Rosnay, P., Dickinson, R. E., Dai, Y. J., Duan, Q. Y., Etchevers, P.,  
609 Henderson-Sellers, A., Gedney, N., Gusev, Y. M., Habets, F., Kim, J. W., Kowalczyk, E.,  
610 Mitchell, K., Nasonova, O. N., Noilhan, J., Pitman, A. J., Schaake, J., Shmakin, A. B.,

611 Smirnova, T. G., Wetzel, P., Xue, Y. K., Yang, Z. L., and Zeng, Q. C.: Effects of frozen  
612 soil on soil temperature, spring infiltration, and runoff: Results from the PILPS 2(d)  
613 experiment at Valdai, Russia, *J. Hydrometeorol.*, 4, 334–351, 2003.

614 McGuire, A.D., Chapin III, F.S., Walsh, J.E. and Wirth, C.: Integrated regional changes in  
615 arctic climate feedbacks: Implications for the global climate system, *Annu. Rev. Environ.*  
616 *Resour.* 31, 61–91, doi:10.1146/annurev.energy.31.020105.100253, 2006.

617 Meehl, G. A., Boer, G. J., Covey, C., Latif, M., and Stouffer, R. J.: The Coupled Model  
618 Intercomparison Project (CMIP), *Bull. Amer. Meteor. Soc.*, 81, 313–318, 2000.

619 Mitchell, T. D., and Jones, P. D.: An improved method of constructing a database of monthly  
620 climate observations and associated high-resolution grids, *Int. J. Climatol.*, 25, 693-712,  
621 2005.

622 Mueller, B., Hirschi, M., Jimenez, C., Ciais, P., Dirmeyer, P. A., Dolman, A. J., Fisher, J. B.,  
623 Jung, M., Ludwig, F., Maignan, F., Miralles, D., McCabe, M. F., Reichstein, M.,  
624 Sheffield, J., Wang, K. C., Wood, E. F., Zhang, Y., and Seneviratne, S. I.: Benchmark  
625 products for land evapotranspiration: LandFlux-EVAL multi-dataset synthesis, *Hydrol.*  
626 *Earth Syst. Sci.*, 17, 3707-3720, doi:10.5194/hess-17-3707-2013, 2013.

627 Muller, J.-P., López, G., Watson, G., Shane, N., Kennedy, T., Yuen, P., Lewis, P., Fischer, J.,  
628 Guanter, L., Domench, C., Preusker, R., North, P., Heckel, A., Danne, O., Krämer, U.,  
629 Zühlke, M., Brockmann, C., and Pinnock, S.: The ESA GlobAlbedo Project for mapping  
630 the Earth's land surface albedo for 15 Years from European Sensors., paper presented at  
631 IEEE Geoscience and Remote Sensing Symposium (IGARSS) 2012, IEEE, Munich,  
632 Germany, 22-27.7.12, 2012.

633 Orth, R., and Seneviratne, S.I.: Analysis of soil moisture memory from observations in  
634 Europe. *J. Geophys. Res. - Atmospheres*, 117, D15115, 2012.

635 Pielke, R.A., Avissar, R., Raupach, M., Dolman, A.J., Zeng, X.B., and Denning, A.S.:  
636 Interactions between the atmosphere and terrestrial ecosystems: influence on weather and  
637 climate, *Glob. Chang. Biol.* 4 (5), 461–475, 1998.

638 Ping, C.L., Michaelson, G.J., Jorgenson, M.T., Kimble, J.M., Epstein, H., Romanovsky,  
639 V.E., and Walker, D.A.: High stocks of soil organic carbon in the North American Arctic  
640 region, *Nat. Geosci.*, 1, 615-619, 2008.

641 Porada, P., Ekici, A., and Beer, C.: Effects of bryophyte and lichen cover on permafrost soil  
642 temperature at large scale, *The Cryosphere Discuss.*, doi:10.5194/tc-2015-223, in review,  
643 2016.

644 Raddatz, T. J., Reick, C., Knorr, W., Kattge, J., Roeckner, E., Schnur, R., Schnitzler, K.-G.,  
645 Wetzel, P., and Jungclaus, J. H.: Will the tropical land biosphere dominate the climate-  
646 carbon cycle feedback during the twenty-first century?, *Climate Dyn.*, doi:  
647 10.1007/s00382-007-0247-8, 2007.

648 Rienecker, M. M., Suarez, M. J., Gelaro, R., Todling, R., Bacmeister, J., Liu, E., Bosilovich,  
649 M. G., Schubert, S. D., Takacs, L., Kim, G.-K., Bloom, S., Chen, J., Collins, D., Conaty,  
650 A., da Silva, A., Gu, W., Joiner, J., Koster, R. D., Lucchesi, R., Molod, A., Owens, T.,  
651 Pawson, S., Pegion, P., Redder, C. R., Reichle, R., Robertson, F. R., Ruddick, A. G.,  
652 Sienkiewicz, M., and Woollen, J: MERRA - NASA's Modern-Era Retrospective Analysis  
653 for Research and Applications, *J. Climate*, 24, 3624-3648, doi:10.1175/JCLI-D-11-  
654 00015.1, 2011.

655 Rudolf, B., and Rubel, F.: Global precipitation, In: Hantel. M. (ed): Observed global climate,  
656 Chap. 11. Landolt–Boernstein: numerical data and functional relationships in science and  
657 technology – new series, Group 5: Geophysics, vol. 6, Springer, Berlin Heidelberg New  
658 York, p 567, 2005.

659 Seneviratne, S. I., and Stöckli, R.: The role of land-atmosphere interactions for climate  
660 variability in Europe, In: *Climate Variability and Extremes during the Past 100 years*,  
661 Brönnimann et al. (eds.), *Adv. Global. Change. Res.*, 33, Springer Verlag. (Book chapter),  
662 2008.

663 Seneviratne, S. I., Lüthi, D., Litschi, M., and Schär, C.: Land-atmosphere coupling and  
664 climate change in Europe, *Nature*, 443, 205-209, 2006.

665 Seneviratne, S. I., Corti, T., Davin, E., Hirschi, M., Jaeger, E. B., Lehner, I., Orlowsky, B.,  
666 and Teuling, A. J.: Investigating soil moisture-climate interactions in a changing climate:  
667 A review, *Earth-Sci. Rev.*, 99, 125-161, doi:10.1016/j.earscirev.2010.02.004, 2010.

668 Serreze, M. C., and Barry, R. G.: Processes and impacts of Arctic amplification: A research  
669 synthesis, *Global Planet Change*, 77, 85-96, doi:10.1016/j.gloplacha.2011.03.004, 2011.

670 Slater, A., Pitman, A., and Desborough, C.: Simulation of freeze thaw cycles in a general  
671 circulation model land surface scheme, *J. Geophys. Res.*, 103, 11303–1131, 1998.

672 Solomon, S., Qin, D., Manning, M., Marquis, M., Averyt, K., Tignor, M. M. B., Miller Jr., H.  
673 L., and Chen, Z. (Eds.): *Climate change 2007: The physical science basis*, Cambridge  
674 University Press, 996 pp., 2007.

675 Stacke, T., and Hagemann, S.: Development and validation of a global dynamical wetlands  
676 extent scheme, *Hydrol. Earth Syst. Sci.*, 16, 2915-2933, doi:10.5194/hess-16-2915-2012,  
677 2012.

678 Stevens, B., Giorgetta, M., Esch, M., Mauritsen, T., Crueger, T., Rast, S., Salzmann, M.,  
679 Schmidt, H., Bader, J., Block, K., Brokopf, R., Fast, I., Kinne, S., Kornblueh, L.,  
680 Lohmann, U., Pincus, R., Reichler, T., and Roeckner, E.: The atmospheric component of  
681 the MPI-M Earth System Model: ECHAM6, *J. Adv. Model Earth Syst.*, 5, 146-172.  
682 doi:10.1002/jame.20015, 2013.

683 Swenson, S. C., Lawrence, D. M., and Lee, H.: Improved simulation of the terrestrial  
684 hydrological cycle in permafrost regions by the Community Land Model, *J. Adv. in*  
685 *Modelling Earth Systems*, 4, doi:10.1029/2012MS000165, 2012.

686 Takala, M., Luoju, K., Pulliainen, J., Derksen, C., Lemmetyinen, J., Kärnä, J.-P., Koskinen,  
687 J., and Bojkov, B.: Estimating northern hemisphere snow water equivalent for climate  
688 research through assimilation of spaceborne radiometer data and ground-based  
689 measurements, *Rem. Sens. Environ.*, 115, doi: 10.1016/j.rse.2011.08.014, 2011.

690 Takata, K., and Kimoto, M.: A numerical study on the impact of soil freezing on the  
691 continental-scale seasonal cycle, *J. Meteor. Soc. Japan*, 78, 199-221, 2000.

692 Taylor, C. M., Birch, C. E., Parker, D. J., Dixon, N., Guichard, F., Nikulin, G., and Lister, G.  
693 M. S.: Modeling soil moisture-precipitation feedback in the Sahel: Importance of spatial  
694 scale versus convective parameterization, *Geophys. Res. Lett.*, 40, 6213–6218,  
695 doi:10.1002/2013GL058511, 2013.

696 Taylor, K. E., Williamson, D., and Zwiers, F.: The sea surface temperature and sea-ice  
697 concentration boundary conditions for AMIP II simulations, PCMDI Report, 60, Program  
698 for Climate Model Diagnosis and Intercomparison. Lawrence Livermore National  
699 Laboratory, Livermore, California, 25 pp., 2000.

700 Taylor, K. E., Stouffer, R. J., and Meehl, G. A.: An overview of CMIP5 and the experiment  
701 design, *Bull. Amer. Meteor. Soc.*, 93 (4), 485-498, 2012.

702 Teuling, A. J., Hirschi, M., Ohmura, A., Wild, M., Reichstein, M., Ciais, P., Buchmann, N.,  
703 Ammann, C., Montagnani, L., Richardson, A. D., Wohlfahrt, G., and Seneviratne, S. I.: A  
704 regional perspective on trends in continental evaporation, *Geophys. Res. Lett.*, 36,  
705 L02404, doi:10.1029/2008GL036584, 2009.

706 Walsh, J. E., Anisimov, O., Hagen, J. O. M., Jakobsson, T., Oerlemans, J., Prowse, T. D.,

707 Romanovsky, V., Savelieva, N., Serreze, M., Shiklomanov, A., Shiklomanov, I.,  
708 Solomon, S., Arendt, A., Atkinson, D., Demuth, M. N., Dowdeswell, J., Dyurgerov, M.,  
709 Glazovsky, A., Koerner, R. M., Meier, M., Reeh, N., Sigurosson, O., Steffen, K., and  
710 Truffer, M.: Cryosphere and hydrology, in: Symon C, Arris L, Heal B (eds.) Arctic  
711 Climate Impact Assessment, Chap. 6: 184-242, Cambridge University Press, 2005.

712 Weedon, G. P., Balsamo, G., Bellouin, N., Gomes, S., Best, M. J., and Viterbo, P.: The  
713 WFDEI meteorological forcing data set: WATCH Forcing Data methodology applied to  
714 ERA-Interim reanalysis data, *Water Resour. Res.*, 50, doi:10.1002/2014WR015638,  
715 2014.

716

717 **Figure captions**

718 Fig. 1 Boreal summer (JJA) precipitation differences [%] relative to WFDEI data for a)  
719 ECH6-REF, b) ECH6-PF, and c) difference between ECH6-PF and ECH6-REF [in  
720 % of WFDEI precipitation].

721 Fig. 2 Boreal summer (JJA) 2m temperature differences [K] to WFDEI data for a) ECH6-  
722 REF, b) ECH6-PF, and c) difference between ECH6-PF and ECH6-REF.

723 Fig. 3 Boreal summer (JJA) surface solar incoming radiation differences [W/m<sup>2</sup>] to CERES  
724 data for a) ECH6-REF, b) ECH6-PF, and c) difference between ECH6-PF and  
725 ECH6-REF.

726 Fig. 4 Catchments of the Baltic Sea and of the six largest Arctic rivers (from left to right:  
727 Mackenzie, Baltic Sea, Northern Dvina, Ob, Yenisei, Lena, Kolyma).

728 Fig. 5 Mean monthly climatology (1989-2009) of discharge (upper panels) and  
729 precipitation (lower panels) over the 6 largest Arctic river catchments (left column)  
730 and the Baltic Sea catchment (land only, right column). Observations comprise  
731 climatological observed discharge and WFDEI precipitation, respectively.

732 Fig. 6 Mean monthly climatology (1989-2009) of evapotranspiration (upper panels) and  
733 relative root zone soil moisture (lower panels) over the 6 largest Arctic river  
734 catchments (left column) and the Baltic Sea catchment (land only, right column).  
735 Evapotranspiration data comprise the mean, minimum and maximum diagnostic  
736 estimates from the LandFlux Eval (LF) dataset. The dashed blue line (PF-Total)  
737 denotes the total root zone moisture content (liquid + frozen) for ECH6-PF.

738 Fig. 7 Mean frozen fraction of total root zone soil moisture (1989-2009) in ECH6-PF over  
739 the 6 largest Arctic river catchments (solid curve) and the Baltic Sea catchment (land  
740 only, dashed curve).

741 Fig. 8 Mean monthly climatological differences (1989-2009) between ECH6-PF and



742 ECH6-REF for precipitation ( $\Delta P$ ) and evapotranspiration ( $\Delta ET$ ) over the 6 largest  
743 Arctic rivers (upper panel) and the Baltic Sea catchment (lower panel). The dashed  
744 lines indicate the corresponding spreads obtained from MPI-ESM simulations of  
745 deVrese et al. (2016).

746 Fig. 9 Mean monthly climatology (1989-2009) of 2m temperature differences to WFDEI  
747 data (upper panels) and surface solar irradiance (SSI; lower panels) over the 6 largest  
748 Arctic river catchments (left column) and the Baltic Sea catchment (land only, right  
749 column). SSI observations comprise CERES data for 2000-2010.

750 Fig. 10 Mean monthly climatology (1989-2009) of surface albedo (upper panels) and snow  
751 pack snow water equivalent (SWE; lower panels) over the 6 largest Arctic river  
752 catchments (left column) and the Baltic Sea catchment (land only, right column).  
753 Albedo observations data from MODIS (2000-2011), CERES (2000-2010) and  
754 GlobAlbedo (1998-2011), SWE observations comprise data from GlobSnow (1989-  
755 2009), MERRA (1979-2013), and SDC climatology.

756 Fig. 11 Chain of processes involved in the soil moisture precipitation feedback over high  
757 latitudes. Red arrows indicate the initiation of the positive feedback loop by the  
758 presence of frozen soil, blue arrows indicate the loop itself.

759 Fig. 12 Correlation of soil moisture and precipitation for a) ECH6-REF, b) ECH6-PF, and c)  
760 difference between ECH6-PF and ECH6-REF.

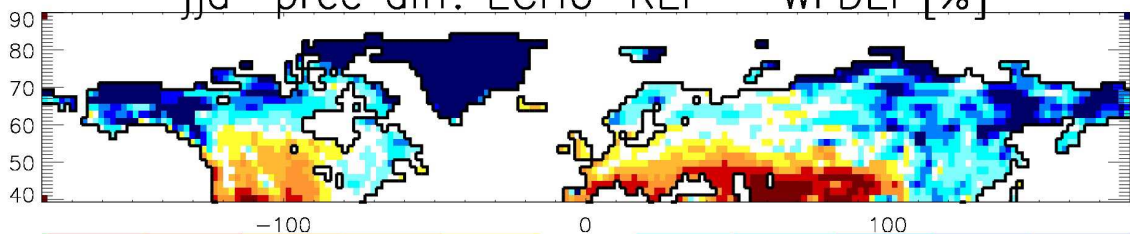
761 Fig. 13 Number of months where in the climatological average of 1989-2009, the upper soil  
762 layer is below 0°C in ECH6-PF.

763

764

a)

jja prec diff. ECH6-REF - WFDEI [%]

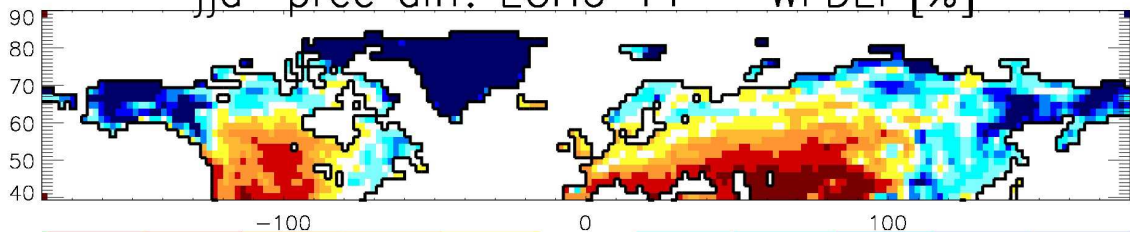


765

766

b)

jja prec diff. ECH6-PF - WFDEI [%]

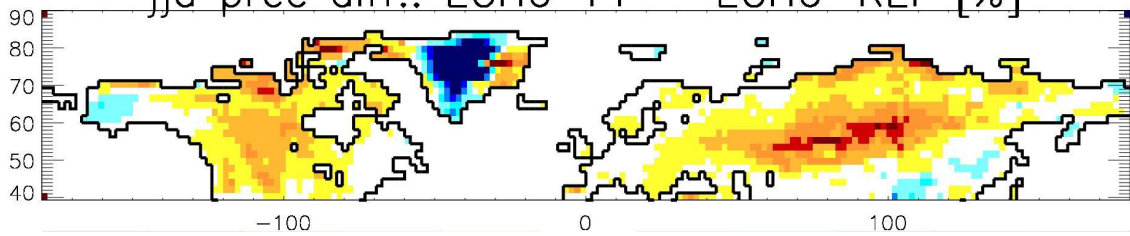


767

768

c)

jja prec diff.: ECH6-PF - ECH6-REF [%]



769

770



771

772

773

774

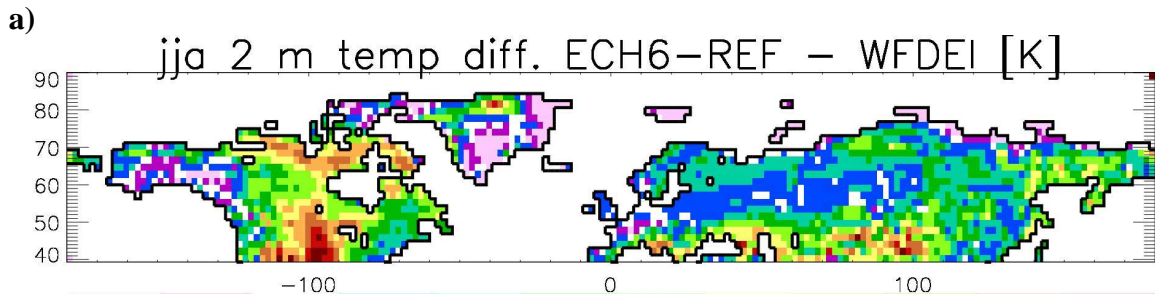
775

**Fig. 1.** Boreal summer (JJA) precipitation differences [%] relative to WFDEI data for a) ECH6-REF, b) ECH6-PF, and c) difference between ECH6-PF and ECH6-REF [in % of WFDEI precipitation].

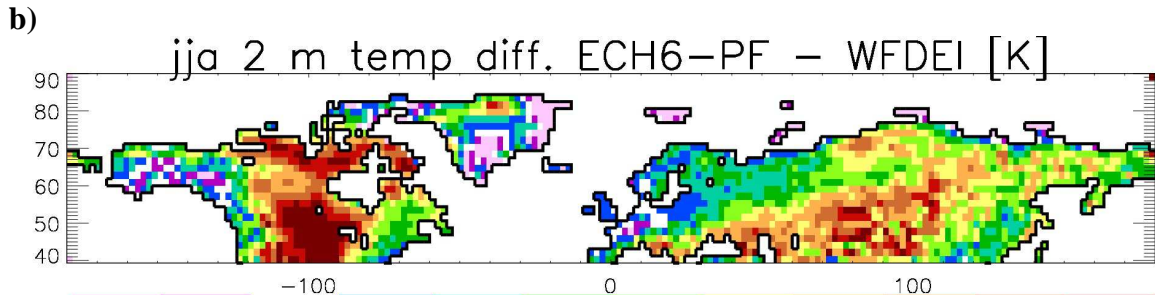
776

777

778

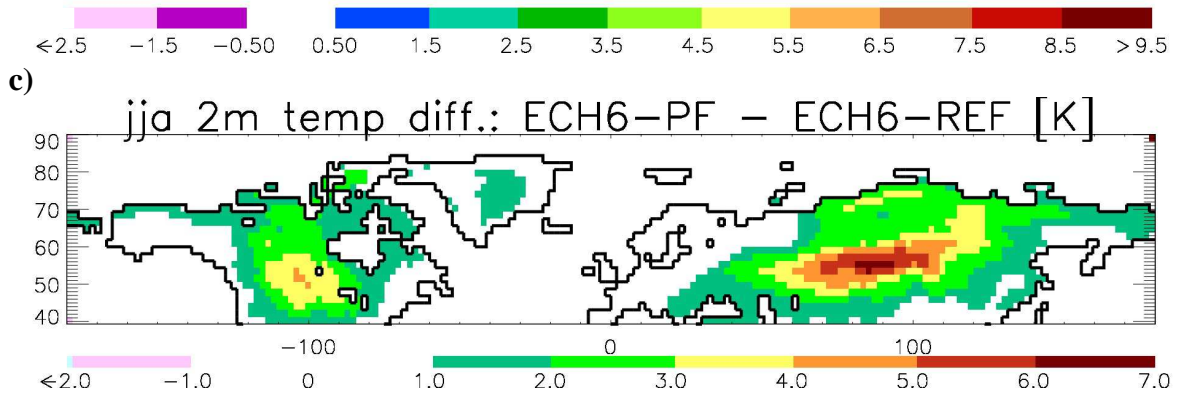


779  
780



781  
782

783  
784

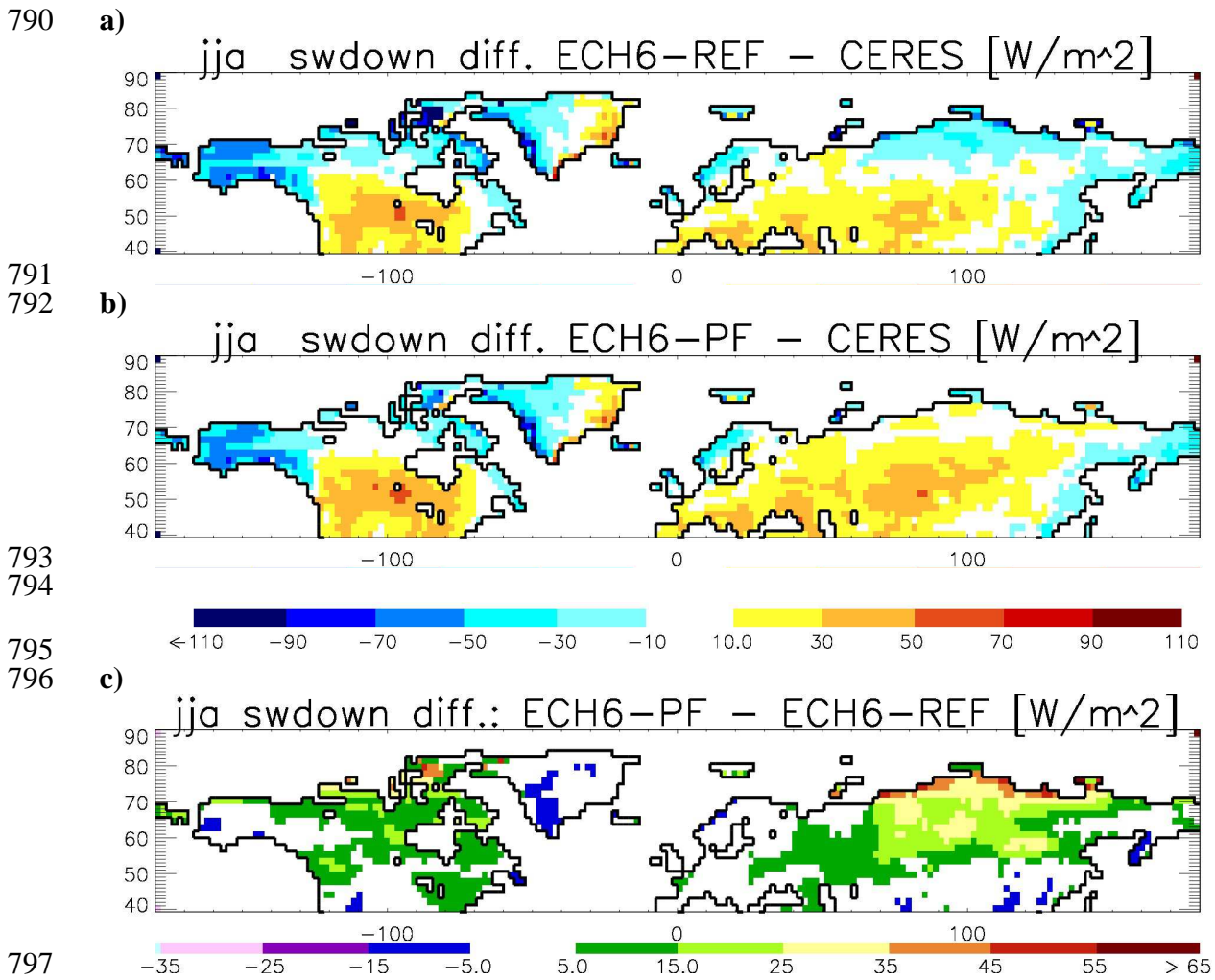


785  
786

787  
788

**Fig. 2.** Boreal summer (JJA) 2m temperature differences [K] to WFDEI data for a) ECH6-REF, b) ECH6-PF, and c) difference between ECH6-PF and ECH6-REF.

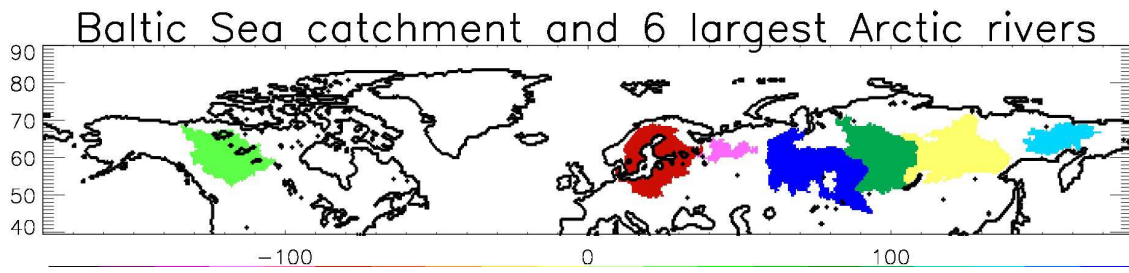
789



797  
798  
799 **Fig. 3.** Boreal summer (JJA) surface solar incoming radiation differences [W/m<sup>2</sup>] to  
800 CERES data for a) ECH6-REF, b) ECH6-PF, and c) difference between ECH6-PF and  
801 ECH6-REF.

802  
803

804  
805

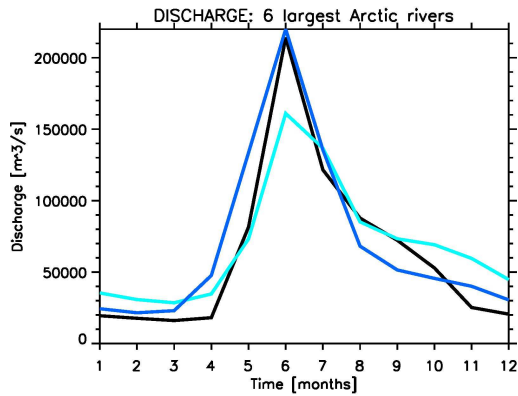


806  
807  
808  
809  
810

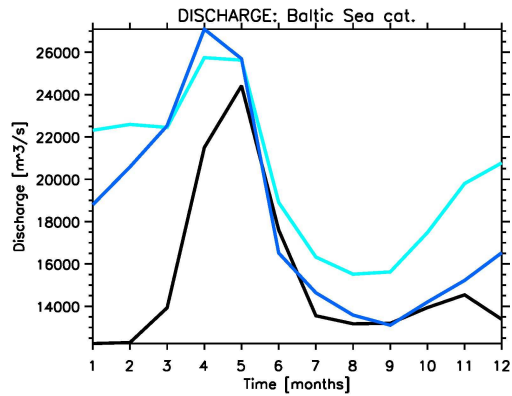
**Fig. 4.** Catchments of the Baltic Sea and of the six largest Arctic rivers (from left to right: Mackenzie, Baltic Sea, Northern Dvina, Ob, Yenisei, Lena, Kolyma).

811  
812  
813  
814

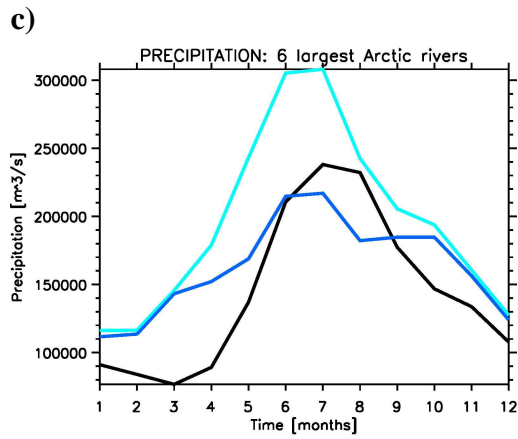
815 a)



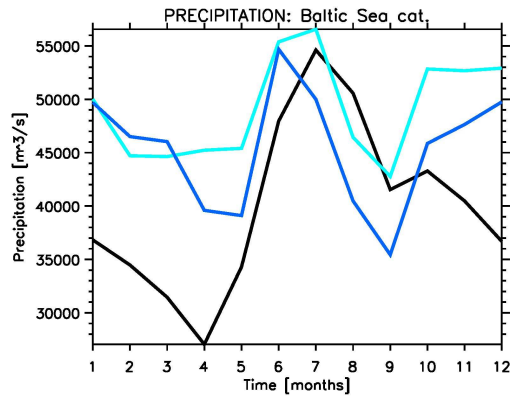
b)



816  
817



d)



818  
819

— Obs.  
— ECH6-REF  
— ECH6-PF

820  
821

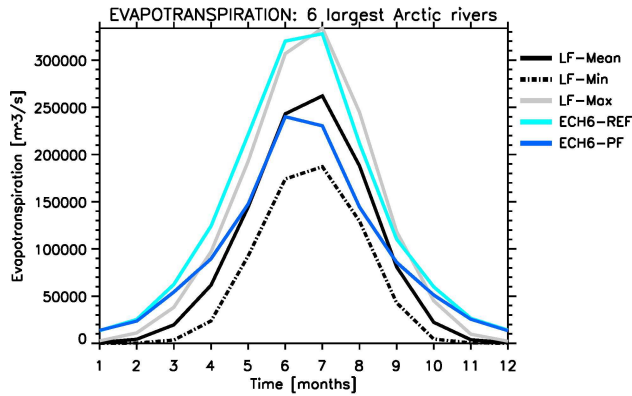
822 **Fig. 5.** Mean monthly climatology (1989-2009) of discharge (upper panels) and  
823 precipitation (lower panels) over the 6 largest Arctic river catchments (left column) and  
824 the Baltic Sea catchment (land only, right column). Observations comprise climatological  
825 observed discharge and WFDEI precipitation, respectively.

826

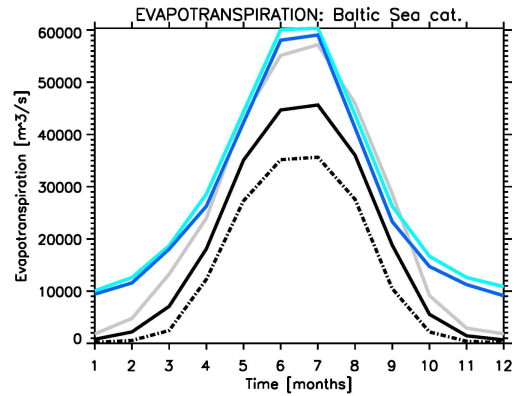
827

828

829 a)

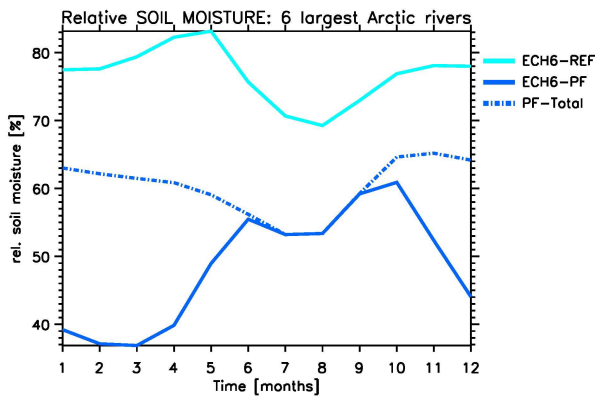


b)

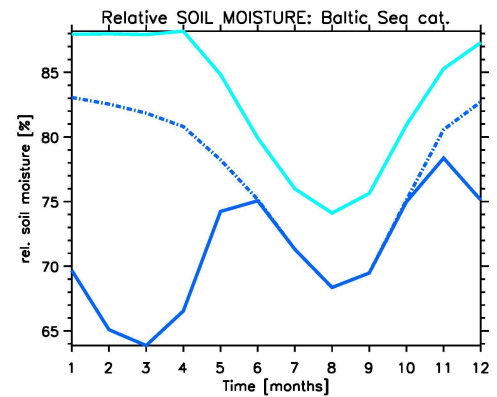


830

831 c)



d)



832

833

834

835

836

837

838

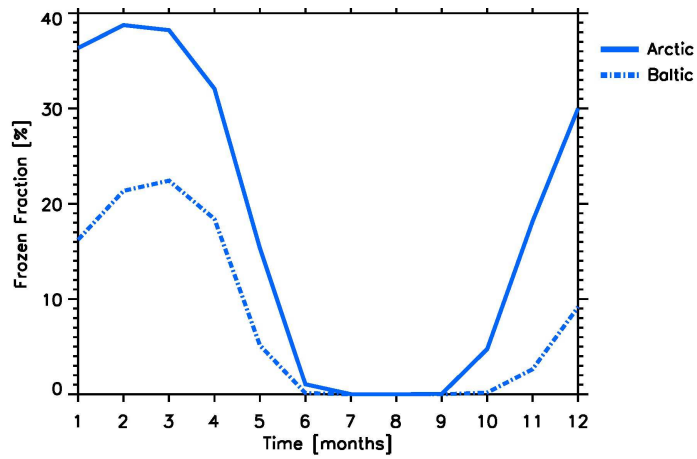
839

**Fig. 6.** Mean monthly climatology (1989-2009) of evapotranspiration (upper panels) and relative root zone soil moisture (lower panels) over the 6 largest Arctic river catchments (left column) and the Baltic Sea catchment (land only, right column). Evapotranspiration data comprise the mean, minimum and maximum diagnostic estimates from the LandFlux Eval (LF) dataset. The dashed blue line (PF-Total) denotes the total root zone moisture content (liquid + frozen) for ECH6-PF.

840

841

842



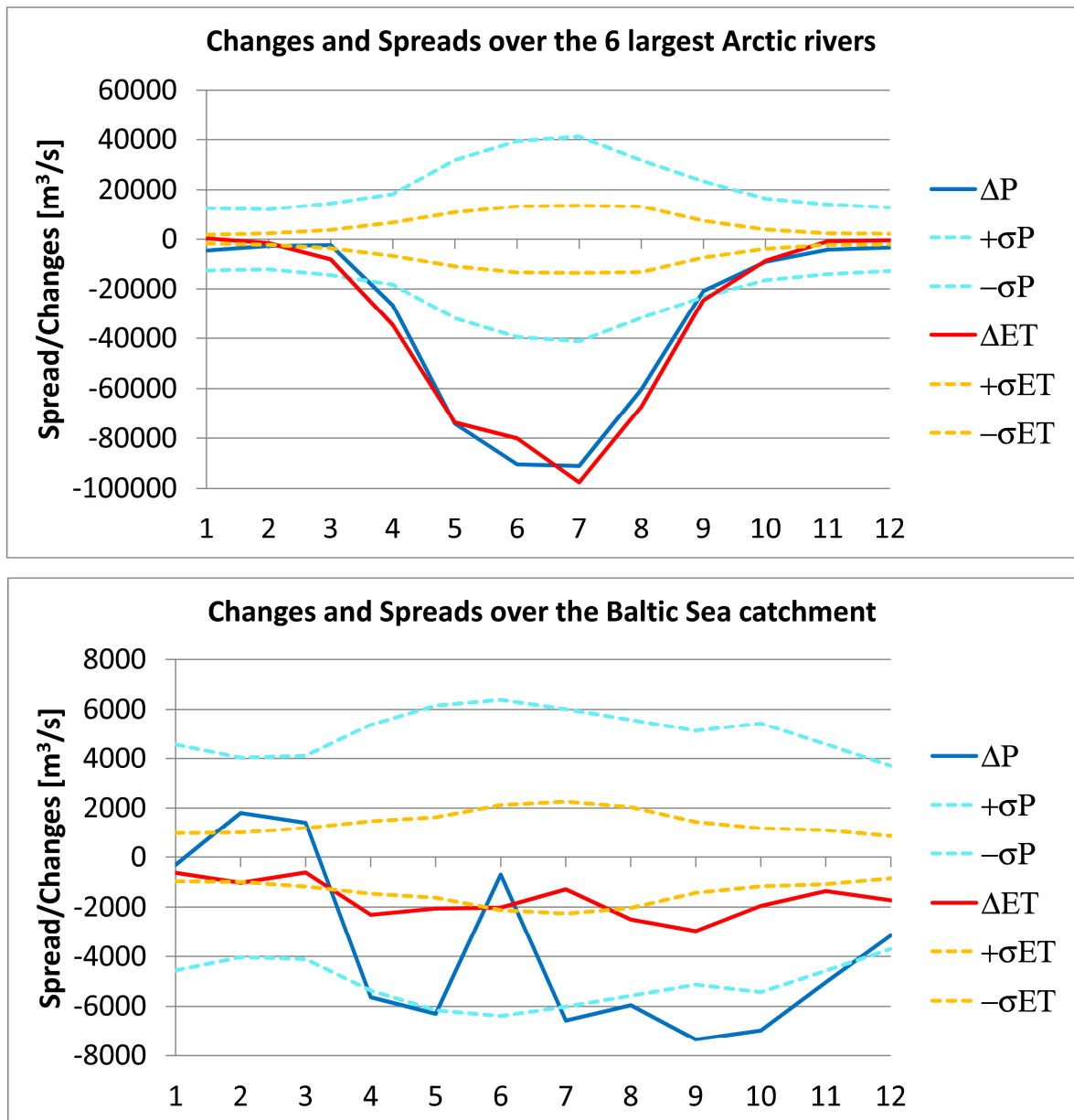
843

844 **Fig. 7.** Mean frozen fraction of total root zone soil moisture (1989-2009) in ECH6-PF  
845 over the 6 largest Arctic river catchments (solid curve) and the Baltic Sea catchment (land  
846 only, dashed curve). Note that for ECH6-REF, this is zero as no freezing is regarded.

847

848





849

850 **Fig. 8.** Mean monthly climatological differences (1989-2009) between ECH6-PF and  
 851 ECH6-REF for precipitation ( $\Delta P$ ) and evapotranspiration ( $\Delta ET$ ) over the 6 largest Arctic  
 852 rivers (upper panel) and the Baltic Sea catchment (lower panel). The dashed lines indicate  
 853 the corresponding spreads obtained from MPI-ESM simulations of deVrese et al. (2016).

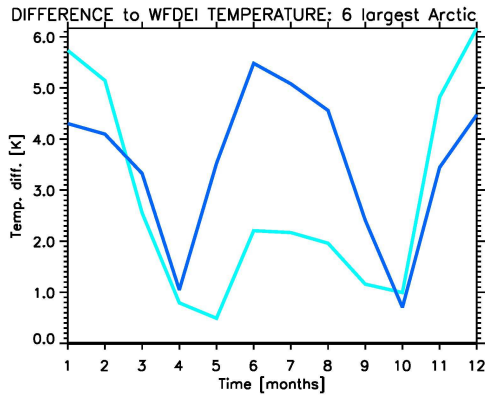
854

855

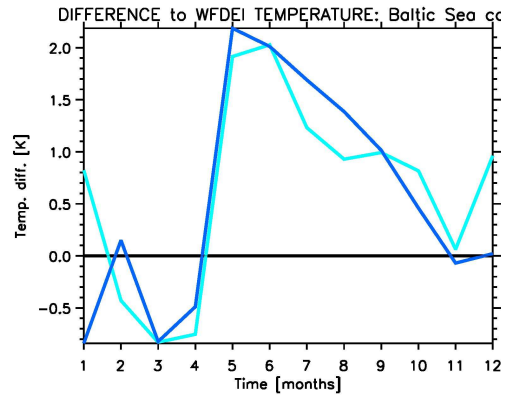
856

857

a)



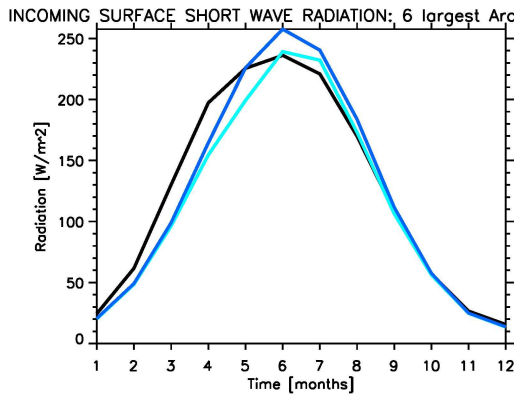
b)



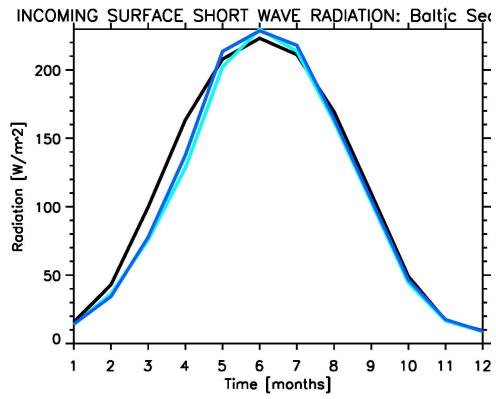
858

859

c)



d)



860

861

— Obs.  
 — ECH6-REF  
 — ECH6-PF

862

863

864

865

866

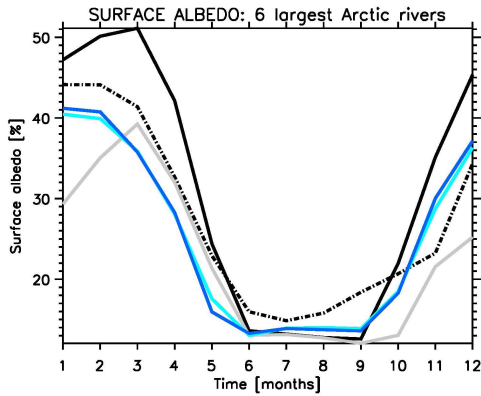
867

**Fig. 9.** Mean monthly climatology (1989-2009) of 2m temperature differences to WFDEI data (upper panels) and surface solar irradiance (SSI; lower panels) over the 6 largest Arctic river catchments (left column) and the Baltic Sea catchment (land only, right column). SSI observations comprise CERES data for 2000-2010.

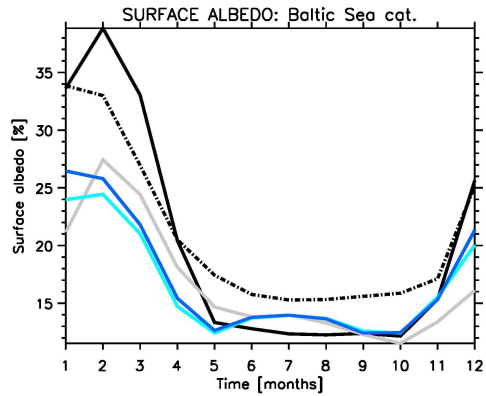
868

869

870 a)

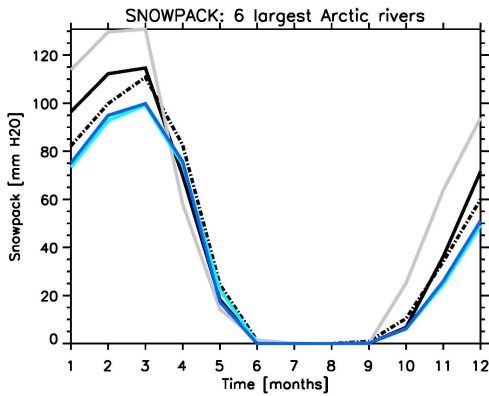


b)

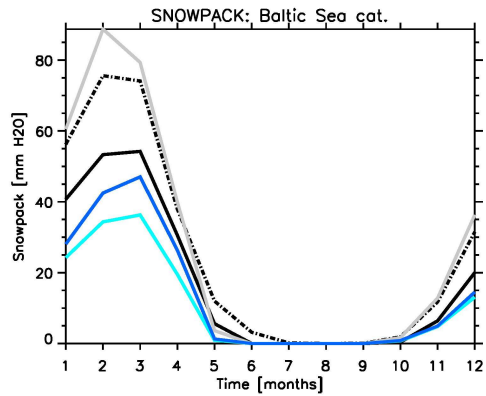


871  
872

c)



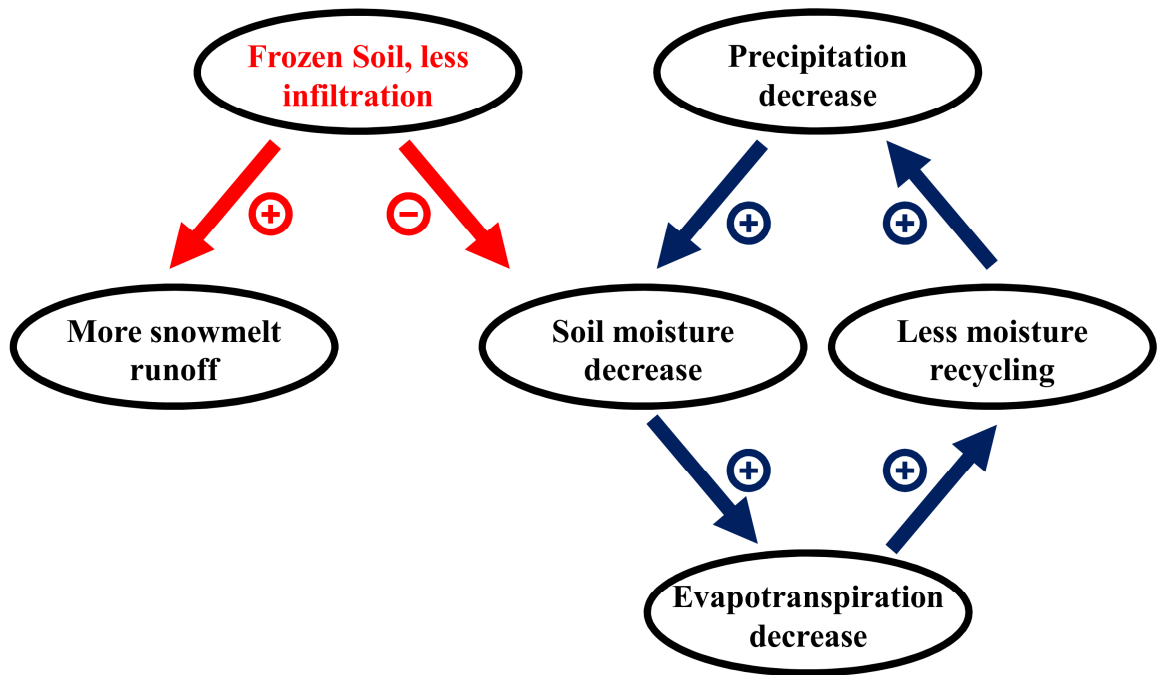
d)



873  
874  
875  
876  
877  
878  
879  
880

**Fig. 10.** Mean monthly climatology (1989-2009) of surface albedo (upper panels) and snow pack snow water equivalent (SWE; lower panels) over the 6 largest Arctic river catchments (left column) and the Baltic Sea catchment (land only, right column). Albedo observations data from MODIS (2000-2011), CERES (2000-2010) and GlobAlbedo (1998-2011), SWE observations comprise data from GlobSnow (1989-2009), MERRA (1979-2013), and SDC climatology.

881



882

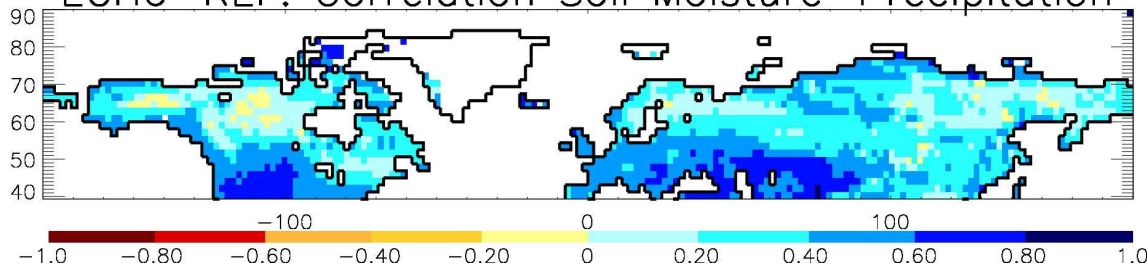
883 **Fig. 11.** Chain of processes involved in the soil moisture precipitation feedback over high  
 884 latitudes. Red arrows indicate the initiation of the positive feedback loop by the presence  
 885 of frozen soil, blue arrows indicate the loop itself.

886

887

888

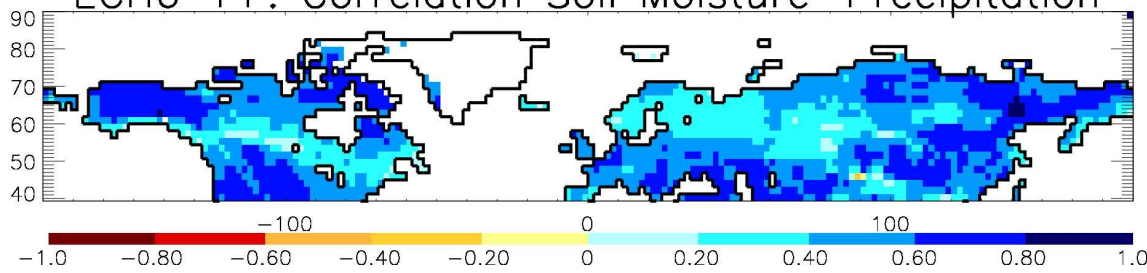
a) ECH6-REF: Correlation Soil Moisture-Precipitation



889

890

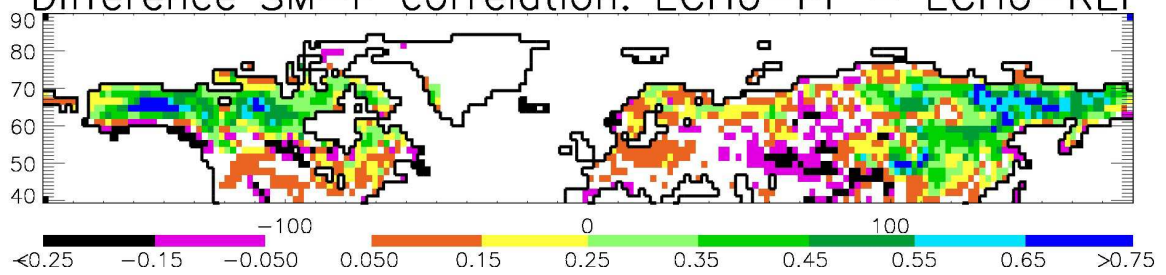
b) ECH6-PF: Correlation Soil Moisture-Precipitation



891

892

c) Difference SM-P correlation: ECH6-PF - ECH6-REF



893

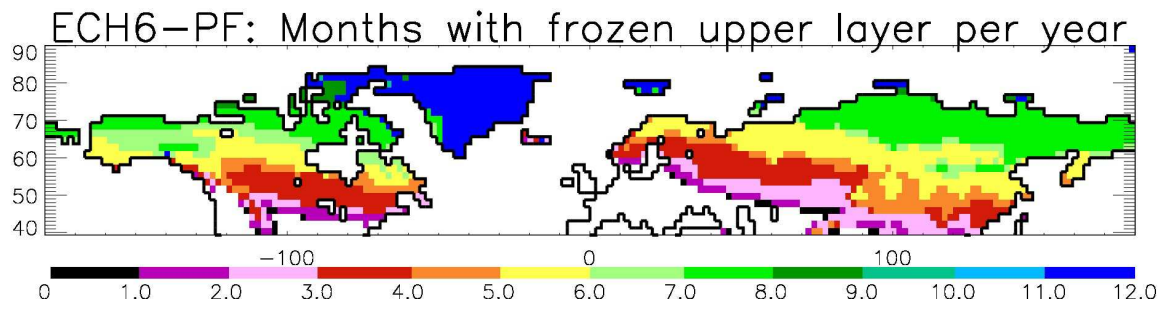
894

895

896

**Fig. 12.** Correlation of soil moisture and precipitation for a) ECH6-REF, b) ECH6-PF, and c) difference between ECH6-PF and ECH6-REF.

897



898  
899  
900  
901

**Fig. 13.** Number of months where in the climatological average of 1989-2009, the upper soil layer is below 0°C in ECH6-PF.

902

903

904 **Table 1.** Summer (JJA) biases over the six largest Arctic rivers for 2m temperature ( $T_{2m}$ , to  
 905 WFDEI), radiative flux ( $R$ ) into the surface due to biases in SSI (to CERES), albedo ( $\alpha$ , to  
 906 GlobAlbedo) and their combined effect (comb.) as well as the estimated related impact on  
 907 surface temperature ( $T_s$ ) and the contribution of the SSI bias to this impact.

Experiment	$\Delta T_{2m}$	$\Delta R$ SSI	$\Delta R$ $\alpha$	$\Delta R$ comb.	$\Delta T_s$ comb.	SSI cont.
ECH6-REF	2.1 K	5.0 W/m <sup>2</sup>	4.1 W/m <sup>2</sup>	9.0 W/m <sup>2</sup>	1.7 K	55%
ECH6-PF	5.0 K	15.8 W/m <sup>2</sup>	4.3 W/m <sup>2</sup>	19.8 W/m <sup>2</sup>	3.6 K	78%

908

909